International Journal of Pharmaceutics 417 (2011) 173–195

Contents lists available at ScienceDirect

International Journal of Pharmaceutics

journal homepage: www.elsevier.com/locate/ijpharm

Quantitative magnetic resonance micro-imaging methods for pharmaceutical research

M.D. Mantle*

Department of Chemical Engineering & Biotechnology, University of Cambridge, Pembroke Street, Cambridge CB2 3RA, UK

ARTICLE INFO

Article history:
Received 28 September 2010
Received in revised form
18 November 2010
Accepted 20 November 2010
Available online 27 November 2010

Keywords:
Micro-imaging
Magnetic resonance
Pharmaceutical
Controlled release
Quantitative

ABSTRACT

The use of magnetic resonance imaging (MRI) as a tool in pharmaceutical research is now well established and the current literature covers a multitude of different pharmaceutically relevant research areas. This review focuses on the use of *quantitative* magnetic resonance micro-imaging techniques and how they have been exploited to extract information that is of direct relevance to the pharmaceutical industry. The article is divided into two main areas. The first half outlines the theoretical aspects of magnetic resonance and deals with basic magnetic resonance theory, the effects of nuclear spin–lattice (T_1), spin–spin (T_2) relaxation and molecular diffusion upon image quantitation, and discusses the applications of rapid magnetic resonance imaging techniques. In addition to the theory, the review aims to provide some practical guidelines for the pharmaceutical researcher with an interest in MRI as to which MRI pulse sequences/protocols should be used and when. The second half of the article reviews the recent advances and developments that have appeared in the literature concerning the use of quantitative micro-imaging methods to pharmaceutically relevant research.

1. Introduction

The use of magnetic resonance imaging (MRI) as a tool in pharmaceutical research dates back to the work of Rajabisiahboomi et al. (1994) who used traditional spin–echo magnetic resonance imaging to investigate the swelling of hydrating hydroxypropylmethylcellulose (HPMC) tablets. Since then there has been a vast amount of work published in the literature concerning the use of magnetic resonance imaging and its application to pharmaceutical systems. Recently, there have been several excellent reviews (Melia et al., 1998; Nott, 2010; Richardson et al., 2005; Zeitler and Gladden, 2009) on the aforementioned subject which, collectively, cover a wide variety of pharmaceutically relevant research. The aim of this review is two fold: (i) to focus on the use of *quantitative* magnetic resonance techniques and how they have been used to extract information that is of direct relevance to pharmaceutical research; (ii) to provide some guidelines for the pharmaceutical researcher with an interest in MRI as to which MRI pulse sequences/protocols should be used and when. The second aim may seem somewhat unusual but there is a good reason for including this. In the last 2–3 years the emergence of commercially available so-called "bench-top" MRI systems has made the use of MRI much more attractive to pharmaceutical research companies, primarily because of the fact that ench-top systems do not require expensive high field superconducting magnets as part of their hardware. In addition, bench-top systems are extremely compact and require only a moderate amount of space in a laboratory. Moreover, a standard United States Pharmacopeia (USP-4) dissolution cell can now be incorporated into a bench-top system (Malaterre et al., 2009; Nott, 2010) and thus permits a direct comparison of MRI data with that from a industry standard USP-4 dissolution apparatus under well defined universally accepted protocols. However, the bench-top phenomenon is still in its infancy in terms of "user friendliness" of the software and MRI pulse programming interfaces, which make the rapid implementation of new techniques cumbersome. Nevertheless, it is likely that bench-top MRI systems will be routinely used by non-MRI specialists in the pharmaceutical industry with increasing frequency, and thus it is prudent to provide some guidelines that will aid the choice of which MRI protocols to use and when.

So, what is meant by "*quantitative*" in terms of magnetic resonance data? One of the defining beauties of the magnetic resonance phenomenon whether it be from an imaging or spectroscopy viewpoint, is that the acquired signal is, in theory, proportional to the number of active nuclei in a particular sample of interest. So in its simplest form magnetic resonance tells us "how much?" of a particular substance we have and thus it can, in principle, be used to spatially map, for example, the concentration of an active pharmaceutical ingredient (API) in a solid dosage form, or the concentration of water or drug in a gel layer. In addition to the question

* Corresponding author. Tel.: +44 1223 347777.
E-mail address: mdm20@cam.ac.uk

0378-5173/$ – see front matter © 2010 Elsevier B.V. All rights reserved.
doi:10.1016/j.ijpharm.2010.11.035

of "how much?", MRI data can also be acquired and manipulated to give quantitative information regarding "how fast? (or indeed how slow?)" molecules of interest move. For example, of particular interest to pharmaceutical research community is quantifying the rate of ingress of dissolution media into swellable matrices, the rate of formation and expansion of gels layers and the rate at which an API is dissolved and subsequently transported from its existence within a gel layer to a surrounding dissolution medium. The answers to the questions of "how much?" and "how fast?" for many pharmaceutically relevant research areas using MRI techniques is sometimes possible, but it is imperative, for the accurate interpretation of data, that the information within the MRI image has been corrected for signal losses that result from so called T_1, and T_2-relxation, diffusion and flow losses. Fyfe and Blazek (1997) and Hyde and Gladden (1998) were amongst the first to note that previous MRI investigations of liquid ingress into polymers were not quantitative as they lacked information from both the liquid and the polymer. Fyfe and Blazek (1997) presented the first fully quantitative study of a pharmaceutically relevant system, namely HPMC swelling by water, using a combination of conventional T_1/T_2 relaxation NMR spectroscopy (for calibration) and T_2 weighted one dimensional non-slice selective imaging/profiling. It is thus timely at this stage to review the basics behind the nuclear magnetic resonance (NMR) and magnetic resonance imaging experiments and highlight some of the more important issues that may cause errors in such measurements of "how much?" of a substance we have and "how fast?" is it moving with a particular focus on the applicability of magnetic resonance micro-imaging methods to pharmaceutical drug delivery systems.

2. Nuclear magnetic resonance (NMR) and MRI theory

The complete theory of NMR and MRI is complex but well established and the reader is referred to several excellent texts on the subject for a thorough treatment (Callaghan, 1993; Haacke, 1999; Levitt, 2001; Liang and Lauterbur, 2000). The basic principles behind the NMR experiment and the origins of T_1 and T_2 relaxation and how they can effect the quantitative interpretation of data are included. In addition, the theory behind spatial resolution in magnetic resonance, to give a magnetic resonance image, as well as the principles behind the magnetic resonance measurement of molecular self-diffusion is considered. A detailed section regarding how the 'imaging' magnetic field gradients, used to give spatial resolution in the first place, may effect quantitation is also included as supplementary material. The aim of this section is not to bore the reader with standard theory that is available in any of the above mentioned texts, but it seeks to provide the experimentalist with the necessary information (in one document) that will allow them to estimate, at least, possible errors associated with quantitative magnetic resonance measurements applied to pharmaceutical research. Finally, each section concludes with some practical guidelines/considerations that may help the experimentalist determine which of the various commonly available MRI methods will provide optimal quantitative magnetic resonance data.

2.1. Nuclear magnetic resonance

Magnetic resonance imaging is essentially a subset of the wider phenomenon of nuclear magnetic resonance. When a nucleus of non-zero nuclear spin is placed in a magnetic field (typically between 1 and 10 T), its nuclear spin energy levels are made non-degenerate. As a result of this, at the equilibrium state of the spin system, there exists a net magnetisation vector aligned parallel to the direction of the magnetic field. By exposing the system to electromagnetic energy of appropriate frequency (radio-frequency

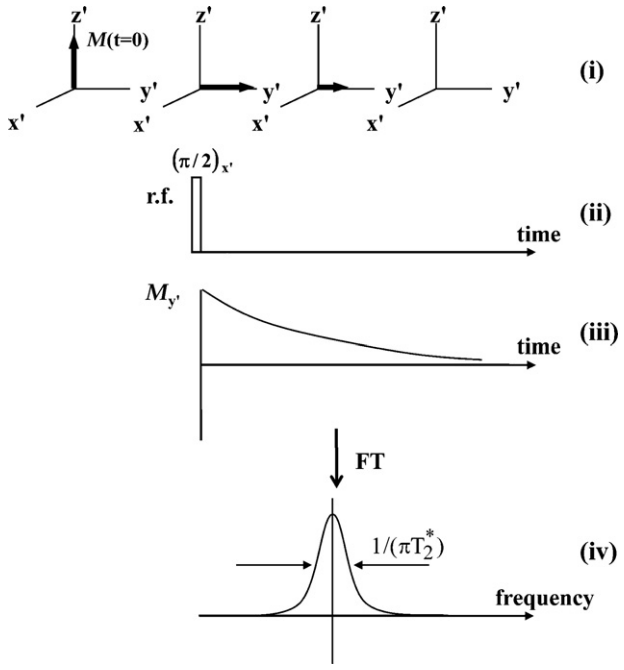

Fig. 1. The behaviour of the magnetisation vector in the rotating frame of reference (i) is shown in response to the application of a single $\pi/2$ r.f. pulse along x', (ii). The decay of the magnetisation vector in the x'–y' plane yields the received time-domain signal, called the Free Induction Decay (FID), shown in (iii). The result of a Fourier transform of the FID is the spectrum shown in (iv). If a liquid state sample is studied the full-width at half-maximum-height of the spectral signal is $1/\pi T_2{}^*$ (see Eq. (1.4)).

(r.f.)), a resonant absorption occurs between these nuclear spin energy levels. The specific frequency at which this resonance occurs is called the resonance frequency and is proportional to the strength of the magnetic field, B_0, used in the experiment. The precise energy level splitting is specific to a given isotope of an element, and the *Larmor* resonance frequency (ω_0) is given by:

$$\omega_0 = \gamma B_0 \tag{1}$$

where γ is the gyromagnetic ratio, which is an isotope-specific property. The precise energy-level splitting is slightly modified by the electronic environment of the nucleus under study, thus ω_0 is also modified and becomes specific to individual molecules containing the element of interest. Thus we can take a spectrum of a mixture of chemical species and identify the presence of particular molecular species in that mixture (i.e. a conventional NMR or MR spectroscopy experiment). As mentioned in the introduction, the measurement is quantitative; i.e. following calibration and allowances for relaxation effects, we know exactly how much of each chemical species is present. A standard way of representing the basic MR measurement is shown in Fig. 1.

Initially, the net magnetisation vector, $\boldsymbol{M}$, is aligned along the direction of the magnetic field. The action of the excitation pulse, in this case a pulse of r.f. applied at right angles (along x') to the direction of the superconducting field is therefore to rotate $\boldsymbol{M}$ about the x'-axis. In this example, the r.f. excitation is applied for sufficient time that $\boldsymbol{M}$ is rotated to lie along the y'-axis in the x'–y' plane. If this condition is met, the r.f. pulse is referred to as a $\pi/2$ (or 90°) pulse; i.e. it has rotated $\boldsymbol{M}$ through $\pi/2$ radians. These processes are actually occurring in the frame of reference of the magnetisation vector (hence the primed symbol) which, in the laboratory frame, precesses about the B_0 axis simultaneously with the action of the excitation pulse. This convention is adopted to simplify the representation of the action of the r.f pulses and, for obvious reasons, is referred to as the 'rotating frame'. In this rotating frame repre-

sentation, the MR time domain signal, following r.f. excitation, is measured by acquiring the signal (i.e. magnitude of the magnetisation vector) aligned along y' as a function of time; this signal will decay with time due to the recovery of the magnetisation along z' and, at shorter timescales, due to the loss of phase coherence of the spin isochromats comprising the net magnetisation vector along the y' axis. These decay processes are termed the spin–lattice (T_1) and spin–spin relaxation (T_2) processes and are key to obtaining quantitative information from the sample of interest; T_1 and particularly T_2 relaxation will be discussed further in the next Section 2.2. The decay of the magnetisation along the y'-axis is recorded as a decaying oscillatory voltage in a receiver coil. Fourier transform of this time-domain signal yields the frequency domain spectral response in which the area under the spectral peak gives a quantitative measure of the number of nuclear spins associated with that spectral frequency (i.e. a quantitative measure of the number of molecules of a given molecular species present). Thus NMR is an intrinsically chemical-specific, quantitative measurement. This is the essential attribute which makes it such a powerful tool in (amongst others) pharmaceutical research.

2.2. Nuclear spin relaxation (T_1 and T_2)

In the following section, the principles of nuclear spin relaxation processes will be summarised and their use in data acquisition discussed. Following the application of the r.f. excitation pulse, the nuclear spin system has excess energy. To return to thermal equilibrium the spin system has to redistribute this excess energy – a process known as "relaxation". A number of different relaxation times characterise different mechanisms for this re-distribution of energy. The most important are the spin–lattice relaxation (T_1) and spin–spin relaxation (T_2) time constants. These time constants characterise the physico-chemical environment of the molecules being studied. T_1, as the name suggests, characterises the energy exchange between the excited spin and the surrounding physical environment (i.e. the lattice), while T_2 characterises entropy-exchange processes within the spin system itself. If a system is characterised by a very rapid T_2 (e.g. many solids) it may not be possible to study it using MRI; this is the major limitation in imaging the solid state. Each chemical species will have its own T_1/T_2 characteristics and these will vary depending on the physical state in which that species exists.

2.2.1. Spin–lattice relaxation, T_1

As shown in Fig. 2, before application of the r.f. excitation pulse the net magnetisation vector, M_0, associated with the nuclear spin system is aligned along the direction of the static magnetic field.

It is the magnitude of this vector that provides the quantitative measurement of the number of nuclear spins excited within the sample. After excitation by a $\pi/2$ r.f. pulse applied along the x' axis, the magnetisation vector is rotated through $\pi/2$ to lie along the y'-axis. As soon as the excitation stops, the systems acts to return to equilibrium; this corresponds to a monotonic increase in the magnitude of the magnetisation vector back along z' as a function of time. If we wait a short time, only a fraction of the magnetisation will have been re-established along z'. If we wait times ~5–7 times longer than T_1, the full magnitude of M_0 will have recovered along z'. The magnitude of the magnetisation vector along z', M_z, as a function of the 'waiting' time, τ, can be written down analytically for any specific r.f. pulse sequence. Eq.(1.1) describes the recovery of the magnetisation back along z' for a saturation recovery pulse sequence:

$$M_z(\tau) = M_0\left[1 - \exp\left(-\frac{\tau}{T_1}\right)\right] \tag{1.1}$$

By recording M_z for a number of τ values and fitting these data to Eq.(1.1), both the T_1 characterising the system and the value of M_0 (which quantifies the number of initially excited spins) are obtained. In a spatially resolved "relaxometry" experiment (i.e. an image), images are acquired at different values of τ, and a fit of Eq.(1.1) to the intensity as a function of τ, for the equivalent pixel, i, in each image allows a complete map of M_{0i} and T_{1i} to be obtained. Thus spatial variation in T_1 can be mapped throughout the image. In practice, the easiest way to avoid having to account (and hence correct) for T_1 relaxation contrast in an image is to ensure that the ones allows at least 3–5 times the longest T_1 relaxation time constant expected in the sample (of course this may have to be measured at some stage) between successive r.f. excitation pulses. Clearly this approach can have its disadvantages in that the total acquisition time of the image, which is essentially governed by the time allowed between successive r.f. excitations for any image protocol where more than one average is required, may become unacceptably long.

2.2.2. Spin-spin relaxation, T_2

On time-scales of less than or equal to that of T_1, spin–spin relaxation (T_2) processes occur. T_2 characterises the loss of phase coherence of the individual spin isochromats in the transverse plane within the spin ensemble comprising the total magnetisation vector M_0. A spin isochromat represents a group of spins which experiences the same homogeneous magnetic field and which therefore behaves in the same way following the excitation pulse. During the period following excitation, the individual isochromats will lose phase coherence with each other as a result of spin–spin interactions and local variations in B_0. The decay of the coherent magnetisation aligned along y', due to spin–spin interactions but not magnetic field heterogeneities, is characterised by the time constant T_2 and measured using a Hahn (1950) spin–echo pulse sequence as shown in Fig. 3.

T_2 is defined as follows:

$$M_y(\tau) = M_0 \exp\left(-\frac{\tau}{T_2}\right) \tag{1.2}$$

With reference to Fig. 3, $\tau = 2t_d$ in Eq.(1.2). The π-pulse acts to reverse the de-phasing effects due to the local heterogeneities in B_0 such that the final acquired signal (the 'echo') suffers attenuation due to spin–spin interactions only. The Hahn spin–echo shown in Fig. 3, has widespread use in MR methods, far beyond simple measurement of T_2. In short, using an echo sequence, instead of exciting the system and then allowing the magnetisation to decay to zero as in Fig. 2, the majority of the magnetisation can be recovered for use in subsequent measurements. The simple Hahn echo sequence shown in Fig. 3 is a common feature of MR imaging pulse sequences. However, one of the problems associated with the measurement of T_2 relaxation times, and hence the back calculation of the true spin population at time $t = 0$ of the species of interest, using the simple Hahn echo sequence is that molecular motion in the form of diffusion (and perhaps flow) can occur during the time interval τ. The (random) diffusion of molecules into spatial regions of different local magnetic field can cause irreversible signal loss in the Hahn echo experiment and thus the measured exponential decay will be faster than expected. This type of behaviour has been well known for a long time and was first realised by Hahn. Eq.(1.2) thus has to be modified to account for diffusion in a linear magnetic field gradient and thus the decay of the excited magnetisation in a single Hahn spin–echo spectroscopy experiment with diffusion in a linear magnetic field gradient (i.e. no spatial imaging gradients) is given by (Callaghan, 1993):

$$M_y(\tau) = M_0 \exp\left(-\frac{\tau}{T_2}\right) \times \exp\left(-\frac{1}{12}\gamma^2 G^2 D(2\tau^3)\right) \tag{1.3}$$

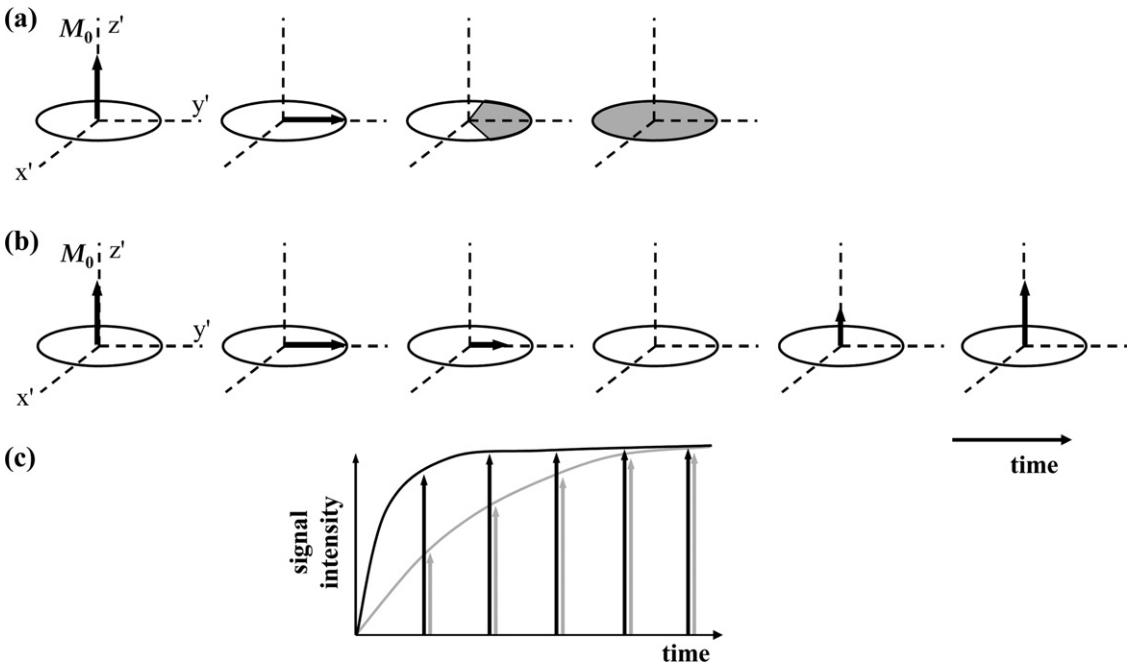

Fig. 2. (a) Similar to Fig. 1, the action of the $\pi/2$ pulse (applied along the x' direction) is to rotate the magnetisation vector into the x'–y' plane, along the y' direction. The individual spin isochromats then dephase in the x'–y' plane, as shown by the increasing size of the shaded region with time. (b) At timescales longer than T_2, the magnetisation recovers back along the direction of the magnetic field B_0, with a characteristic time constant T_1. (c) Two different species within the same sample may have different characteristic T_1 values. In this example, the species associated with the black arrows has a shorter T_1 than the species associated with the grey arrows; the arrows indicate the magnitude of the acquired signal intensity following the initial r.f. excitation. If data are acquired at long times after r.f. excitation, equal signal intensity will be acquired from both species. However, if data are acquired very soon after the excitation pulse, the acquired signal will be predominantly associated with the species characterised by the shorter T_1. This illustrates the principle of relaxation contrast.

where G is the magnitude of the magnetic field gradient strength and D is molecular self-diffusion coefficient of the species being studied. The influence of molecular diffusion in linear magnetic field gradients on the measurement of T_2 relaxation times may be minimised by adopting the so called Carr, Purcell, Meiboom and Gill (Carr and Purcell, 1954; Meiboom and Gill, 1958) T_2 measurement which is essentially a repeated Hahn spin–echo consisting of a series of 180° refocusing pulses that are phase shifted by 90° from the initial excitation pulse. The delay between the initial r.f. excitation pulse and the 180° refocusing pulse is kept to a minimum to minimise the diffusive signal losses during the successive refocusing periods. Thus the CPMG T_2 experiment is a better reflection of the true T_2 relaxation time of a sample than the simple Hahn echo experiment. However it is often insightful to acquire both sets of data from a sample as the difference between the two measurements can give an indication of the magnitude of the background magnetic field gradients (Hurlimann, 1998) that may be present in the sample of interest which can, in turn, affect the interpretation of imaging data.

An additional and important relaxation time constant is T_2^* which characterises a faster decay of the magnetisation along y' and includes the additional effects of magnetic field heterogeneities on

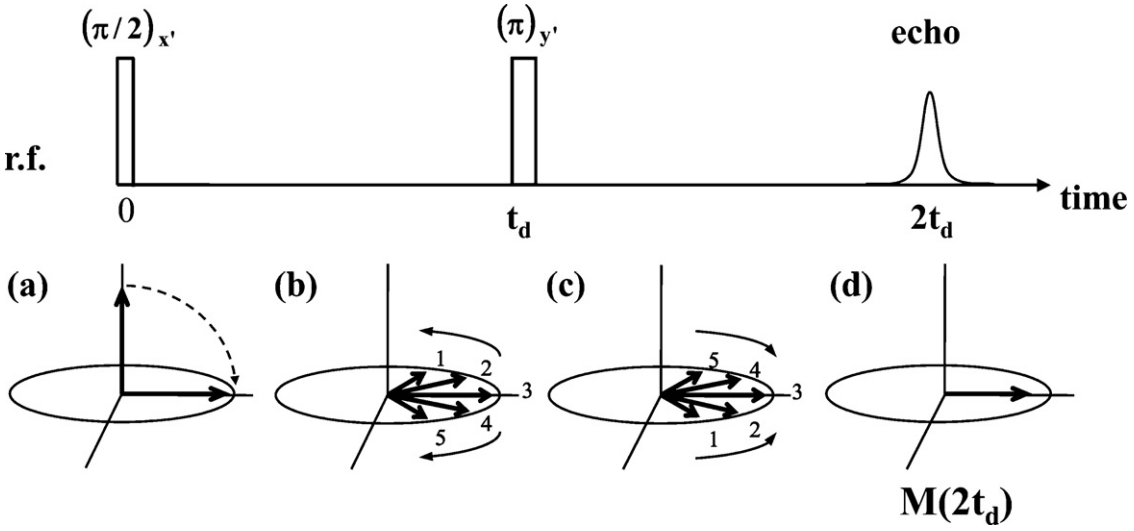

Fig. 3. A Hahn spin–echo pulse sequence used to determine T_2. (a) A $(\pi/2)_{x'}$ pulse puts M_0 into the y'-direction, and (b) the spin isochromats dephase with time. At a time t_d later, a π pulse is applied along the y'-axis causing the spins to 'refocus' (c) along the y'-axis to form an 'echo' (d) at time $2t_d$. The decrease in magnitude of the magnetisation vector between stages (a) and (d) provides a measure of T_2 (Eq. (1.2)). All 'reversible' contributions to the T_2 process are removed by the application of the π pulse.

the loss of phase coherence of the magnetisation following excitation. The simple pulse-acquire sequence (with no refocusing) shown in Fig. 1 gives a time-domain response in which the envelope of the decay in the time domain and hence the width, $\Delta\nu$, of the frequency domain signal is characterised by:

$$T_2^* = \frac{1}{\pi\Delta\nu} \tag{1.4}$$

3. Magnetic resonance imaging

So far, the discussion on NMR theory has been limited to spectroscopic measurements, i.e. ones that are made on the whole sample. This type of measurement has been, and still is, the staple diet of chemists and biochemists whose common goal is essentially to determine the structure, bonding and dynamic properties of molecules. To continue, we will need to introduce the theory behind the formation of an *image* from a sample, i.e. how can we obtain local, as opposed to whole or bulk, information from a sample of interest?

Consider a 20 mm outer diameter glass tube filled to 2.0 cm depth of water which resides at the center of a 7.05 T superconducting magnet, surrounded by a 25.0 mm r.f. coil which in turn is surrounded by a shielded gradient system capable of producing a maximum gradient strength of 1 T m^{-1} (100 G cm^{-1}) in each of 3 orthogonal directions. As we have seen a simple Hahn spin–echo r.f. pulse sequence applied to the ^{1}H nuclei within the sample will, upon Fourier transformation and phase correction, yield a single narrow line at the basic Larmor frequency (Fig. 4a).

Spatial resolution of the water sample may be achieved by the combination of magnetic field gradients in say the z-direction, which are inserted between $\pi/2$ and π pulse and during the acquisition according to Fig. 4b. Now, acquisition takes place under the application of a gradient in the magnetic field in the z-direction. The resulting frequency spectrum or *image* now contains a range of Larmor precession frequencies, which depend upon the magnitude of the applied gradient and the position of the individual water nuclear magnetic moments in the sample tube. Mathematically, the resonance frequency of a nuclear spin in the 1D-profiling experiment may be written as:

$$\omega(\mathbf{r}) = \gamma(B_0 + \mathbf{G}\cdot\mathbf{r}) \tag{1.5}$$

where $\omega(\mathbf{r})$ is the resonance at position $\mathbf{r}$ in the sample, γ the gyromagnetic ratio of the nucleus under study, B_0 the magnitude of the external magnetic field and $\mathbf{G}$ the gradient of the linear applied magnetic field gradient vector. If now we consider the local volume element dV within our tube of water the local spin density, $\rho(\mathbf{r})$, for spins within the volume element dV is then $\rho(\mathbf{r})$dV. The NMR signal from this element may then be written as:

$$dS(\mathbf{G}, t) = \rho(\mathbf{r})\exp[i\omega(\mathbf{r})t]d\mathbf{r} \tag{1.6}$$

Inserting Eq. (1.5) into Eq. (1.6) we obtain:

$$dS(\mathbf{G}, t) = \rho(\mathbf{r})\exp[i(\gamma B_0 + \gamma\mathbf{G}\cdot\mathbf{r})t]d\mathbf{r} \tag{1.7}$$

Obviously at this stage we have neglected to include any relaxation effects and thus the dephasing of the magnetisation is due purely to the term in the exponent of Eq. (1.7). A transformation into the rotating frame of reference followed by explicit integration over all space of allows us to write Eq. (1.7) in terms of the observed signal S as a function of time and therefore becomes:

$$S(t) = \iiint \rho(\mathbf{r})\exp[i\gamma G\cdot\mathbf{r}t]d\mathbf{r} \tag{1.8}$$

where the symbol $d\mathbf{r}$ represents integration overall all space. Mansfield and Grannel (Mansfield and Grannell, 1973) simplified the meaning of Eq. (1.8) by introducing the concept of k-space (the bold face type for k is now dropped for convenience), which may defined by:

$$k = \frac{\gamma Gt}{2\pi} \tag{1.9}$$

The k-space vector units are in reciprocal space units, i.e. m^{-1} and thus the inverse of the maximum k-space vector is equal to the inherent volume element or voxel resolution of the system. Clearly, values of k-space may be traversed by either varying the time for which the magnetic field gradient is applied or by varying the amplitude of the magnetic field gradient. Inserting the expression for the reciprocal space vector k given in Eq. (1.9) into Eq. (1.8) gives an expression which relates the time domain signal, i.e. that which is actually acquired in an MRI experiment as:

$$S(\boldsymbol{k}) = \iiint \rho(\mathbf{r})\exp[i2\pi k\cdot\mathbf{r}]d\mathbf{r} \tag{1.10}$$

The NMR signal that is acquired in the time domain is in reciprocal space and is generally non-intuitive. Hence it is commonplace to interpret NMR data in the frequency domain. Fourier transformation of the above equation gives:

$$\rho(\mathbf{r}) = \iiint S(\mathbf{k})\exp[-i2\pi k\cdot\mathbf{r}]\,d\mathbf{k} \tag{1.11}$$

Taken together, Eq. (1.10) and Eq. (1.11) tell us that S($\boldsymbol{k}$) and $\rho(\mathbf{r})$ form a mutually conjugate Fourier transform pair. In order for a fully resolved image to be acquired at the desired field-of-view and spatial resolution it is necessary to traverse and acquire all desired points in k-space. For this reason k-space is useful in designing and explaining magnetic resonance imaging pulse sequences. The material presented in Supplementary material section A.1 discusses in more depth the principles behind k-space and how a two-dimensional image is formed in terms of k-space trajectories.

3.1. The effect of random molecular motion on image contrast: self-diffusion

Section 2.2.2 indicated that molecular motion in the form of diffusion can have an adverse effect on a magnetic resonance signal. Before we examine how molecular self-diffusion can affect image contrast and quantitation, we will briefly describe the principle behind the magnetic resonance measurement of self-diffusion phenomena. Magnetic resonance techniques can be exploited to measure molecular self-diffusion coefficients, which are essential transport parameters. We do note at this point that we are exclusively talking about the measurement of the molecular *self-diffusion* coefficient, which implies that the system of interest is at true equilibrium, i.e. there is no gradient in chemical potential in the system to cause a next flux of molecules in a particular direction. If a gradient in chemical potential does exists then the *transport* (sometimes known as Fickian) diffusion can also be determined from an analysis of magnetic resonance imaging data. In this situation the *approach* to either steady state or equilibrium is captured by MR techniques and the data is then usually fitted to an appropriate mathematical model and mass balance with suitable boundary conditions to extract the transport diffusivity. Examples of both types of measurement will be given later. The principle behind the measurement of self-diffusion coefficients using magnetic resonance is as follows.

The formation of a Hahn spin–echo during a pulse sequence containing magnetic field gradient pulses (see Fig. 4b) assumes that the individual nuclei in the sample experience the same local Larmor precession frequencies during the de-phasing and re-phasing gradient components of the pulse sequence. Put simply, we assume that the individual magnetic moments in the spin system under study do not physically move in a magnetic field gradient during

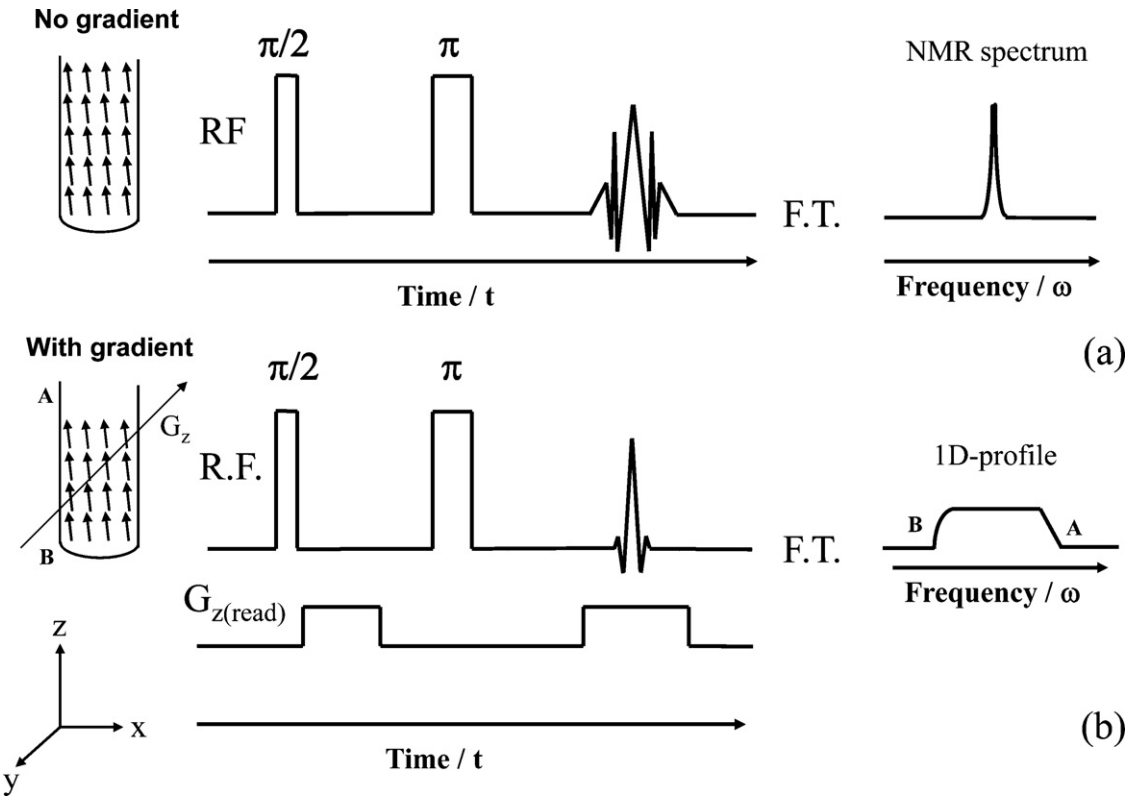

Fig. 4. (a) A Hahn spin–echo applied to a water sample and its resulting ^{1}H NMR spectrum. (b) A simple 1D-imaging profile spin–echo sequence applied to the sample in the *z*-direction.

an NMR experiment. Obviously this is not the case for most systems studied using magnetic resonance as molecular self-diffusion is always present and significant background magnetic field gradients are common in many physical systems. This type of motion causes random fluctuations of the Larmor frequency of the individual magnetic moments within the spin system and thus any signal acquired is now a complex superposition of pulse sequence imparted frequency/phase encoded signal and that due to the residual phase shifts resulting from random motion. The experimental determination of molecular self-diffusion coefficients by magnetic resonance is achieved by the application of a simple pulsed (magnetic) field gradient spin–echo (PFG-SE) as first realised by Stejskal and Tanner (1965). This experiment consists of a standard r.f. $\pi/2 - \pi -$ spin–echo with the additional incorporation of a pair of pulsed magnetic field gradients of duration δ, amplitude G, with a time between the centers of the pulsed magnetic field gradients of Δ, either side of the $\pi-$r.f. refocusing pulse (see Fig. 5).

In practice, the NMR signal is acquired for different values of the pulsed magnetic field gradient strength G whilst keeping the durations, δ and Δ constant. The measured NMR signal intensity, I, is then plotted as a function of the gradient strength G and a numerical fit of the data according to:

$$\frac{I}{I_0} = \exp\left(-\gamma^2\delta^2G^2D\left(\Delta - \frac{\delta}{3}\right)\right) \tag{1.12}$$

is then performed. A plot of the logarithm of the signal intensity versus $-\gamma^2\delta^2G^2(\Delta\text{-}\delta/3)$ will yield a straight line (for Brownian diffusion) whose gradient is the self-diffusivity D. The interpretation and measurement of NMR data for systems exhibiting random (Brownian) diffusion is simple enough, but a more complex behaviour of the signal intensity is often observed in non-Brownian systems.

The method just described was a description of how molecular self-diffusion could be measured using PFG-NMR from the whole sample. A spatially resolved *diffusion image*, i.e. one where a map of self-diffusion coefficients from each individual pixel within an image can be extracted, is easily acquired by preconditioning a standard spin–echo (or gradient echo)(Callaghan, 1993) imaging sequence with a varying amount of diffusion weighting. One thus obtains a data set that contains several images (usually at least eight) with a different amount of diffusion weighting between each image. The intensity of each pixel in the image is then extracted and fitted to the Stejskal and Tanner (1965) (Eq. (1.12)) to obtain the diffusion map. Diffusion weighted imaging (DWI) as it is more commonly known, is an important tool in clinical research and has also been exploited in the pharmaceutical research. The experimentalist must be aware that the magnetic field gradients used to obtain the spatial image can also complicate the contrast in a standard spin–echo or gradient echo image in other ways. Brandl and Haase (1994) were the first to show some of the pitfalls associated with standard spin–echo imaging sequences and molecular diffusion, especially in micro-imaging situations. In particular they came to the conclusion that the signal-to-noise ratio and T_2 relaxation time in ^{1}H NMR microscopy was strongly affected by diffusion. Their results have some important consequences for quantitative MRI in pharmaceutical research as one often seeks resolutions in the 10–100's of microns range which inevitably warrants the use of high, B_0-field systems, for better signal-to-noise ratios, and high magnetic field gradient strengths required for high spatial resolution. A detailed discussion of Brandl and Haase (1994) works is included in Supplementary material section A.2.

As mentioned at the start of this article one of the aims of this article is to provide some general guidelines for experimentalists using MRI in pharmaceutical research to obtain quantitative information from their image data. The following points summarise what has been said so far:

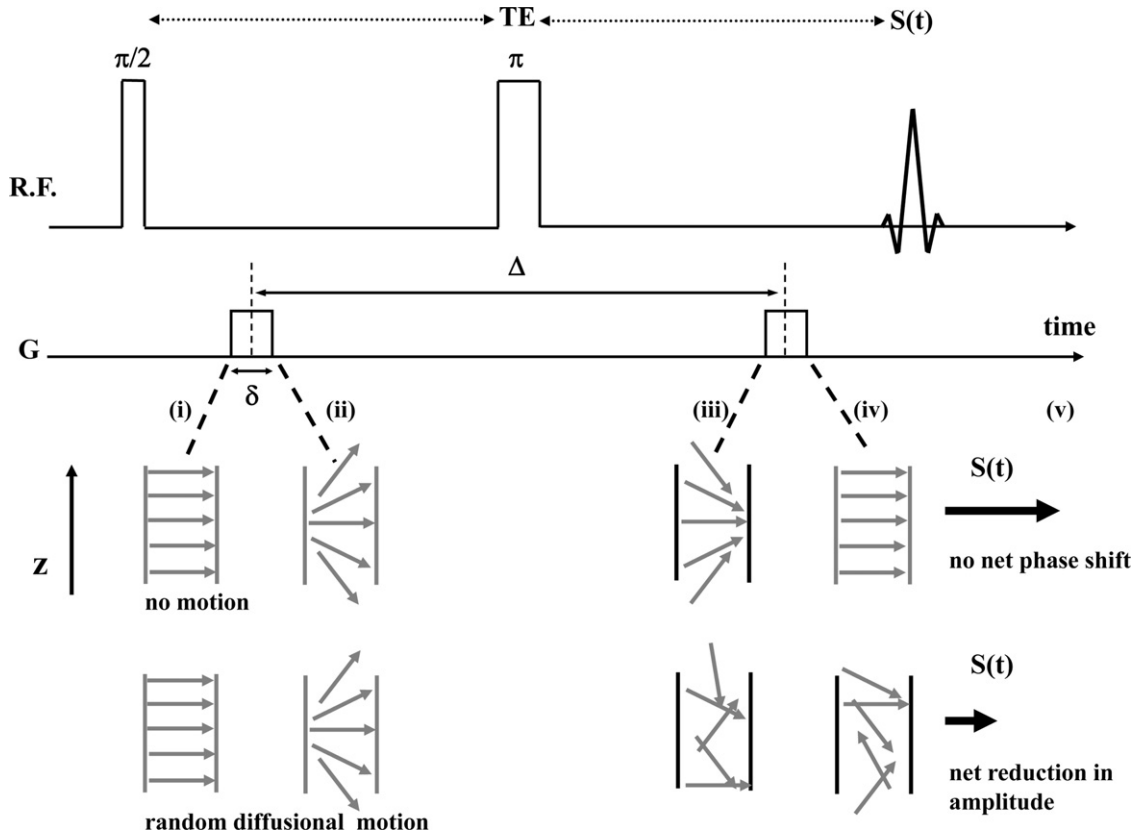

Fig. 5. The principle of transport measurements using the 'phase shift' approach. Two pulsed magnetic field gradients (of magnitude G and duration δ) are applied a time Δ apart. The action of the first pulsed magnetic field gradient is to introduce a phase shift to each nuclear spin with respect to its orientation if no field gradient were to have been applied. The phase offset non-invasively 'labels' the position of the nuclear spin. A 180° refocusing pulse then inverts the phase of the spins. At a time Δ later, the spin system receives an equal pulsed magnetic field gradient. If the spins have not moved, the spins receive an equal and opposite phase offset and return to their initial alignment in the x'–y' plane. Incoherent motion (i.e. diffusion and dispersion) causes a loss of alignment of the nuclear spins within the sample; the resulting attenuation in the received signal provides a measure of the distance travelled by the ensemble of spins during the observation time, Δ. The figure shows the relative phase offset of 5 adjacent spin isochromats, initially lying at different locations along the direction of the applied pulsed magnetic field gradients: (i) after r.f. excitation and before application of the first gradient pulse the spin isochromats are aligned along y'; (ii) immediately after application of the first gradient pulse; (iii) after the system has been phase inverted by the 180° refocusing pulse it then is allowed to evolved for the time Δ; (iv) after application of the second gradient pulse. (v) represents the resulting net magnetisation vector characterising the system after application of the two gradient pulses.

(1) To avoid T_1 relaxation contrast in the image (or having to correct for it), ensure that the recycle time of the experiment is 3–5 times the longest T_1 of the sample. Be aware that this may change dramatically through the course of an experiment.
(2) For simple spin–echo imaging use a minimum echo time (TE) to minimise T_2 contrast within the image.
(3) For quantitative imaging of spin–density (assuming (1) above holds) where a series of T_2 weighted images are acquired; use a modified spin–echo sequence as described by Hsu et al. (1995) to minimise overall signal diffusive losses associated with the imaging gradients themselves. Alternatively, to minimise diffusive losses in background magnetic field susceptibility gradients a T_2-CPMG (Carr and Purcell, 1954; Meiboom and Gill, 1958) preconditioning sequence should be used prior to the spatial imaging sequence.
(4) Estimate[1] signal diffusive losses for a spin–echo imaging sequence by calculating the value of expected signal attenuation of the re-phasing frequency encoding read gradient using:

$$(\%)\,\text{Signal Loss} = 1 - \exp\left[-\frac{D\pi^2}{\Delta x^2}\left(TE - \frac{2}{3}AQ\right)\right] \quad (1.13)$$

[1] The formulas and meanings of the symbols to calculate these losses accurately are given in supplementary material section [A.2].

4. Rapid imaging techniques

Sections 3.0 and A.1 discussed how an image was formed in a magnetic resonance experiment by the simultaneous use of r.f. pulses and magnetic field gradients. It was also stated in Section 2.2.1 that in order to avoid T_1 relaxation contrast the magnetisation in any magnetic resonance experiment should be recycled in a time three to five times greater than the longest T_1 relaxation constant in the sample to give data that is between 95% and 99.9% T_1 contrast free respectively. However, the downside of this imaging method is that it can take a long time to acquire. For example, a typical slice selective transverse xy-image data set would consist of 128×128 data points in the read (x) and phase (y) encoded directions. In general, the total image acquisition time is given by the product of the number of signal averages (NA), the number of phase encoded points ($N.p.e.$) and the recycle time (TR) of the experiment. Of course, one also needs to know the values of the longest T_1 relaxation time of the sample under investigation. Water has a relaxation time of around 2.5 s in a 4.7 T magnet and thus the total image acquisition time for $NA = 2$, $N.p.e. = 128$ and $TR = 7.5$ s is equal to approximately 32 min. This time may be unacceptably long if the system under investigation is changing on the order of seconds or minutes. Moreover, the T_2- relaxation time also needs to be accounted for to obtain a T_1/T_2 relaxation contrast free image. Therefore, to characterise the T_2 relaxation time behaviour of an image one would need to acquire eight sets of T_2 weighted images

and thus acquisition time for such an experiment has now increase from 32 minutes to 4.3 hours! So, how do we speed up our image acquisition time without compromising the quantitative nature of the contrast present in the image?

In general, the acquisition speed of an MR image may be improved by two basic methods:

1. The sampling of more than one line of *k*-space for each r.f. excitation of the spin system.
2. The use of rapid multiple r.f. excitations (and subsequent acquisitions).

4.1. Echo planar imaging (EPI)

The first example of rapid *k*-space imaging was demonstrated by Mansfield (1977) who realised that a complete image could be formed by the acquisition of multiple lines in *k*-space following a single r.f. excitation in a technique today known as echo planar imaging (EPI). In common with many modern fast imaging sequences, the technique relies on the refocusing and acquisition of signal after an initial line in *k*-space has been acquired. In traditional imaging sequences each excitation would give rise to the acquisition of a single line of data in *k*-space after which the signal was not recovered and the magnetization was allowed to return to the *z* direction. Mansfield and Grannell (1973) realised that the magnetization after acquisition of the initial line in *k*-space could be refocused and used to acquire further information, i.e. more lines of data in *k*-space or more averages of the same line in *k*-space. In the case of EPI this is achieved with successive *gradient refocused* or gradient echoes. There are many variants of EPI imaging these days to try to ensure reliable imaging with what is a relatively 'fragile' sequence. A standard blipped EPI sequence (Howseman et al., 1988) to acquire a 128×128 data point image from initial excitation to the end of complete acquisition, incorporating an acquisition bandwidth of 100,000 Hz with gradient rise times of around 100 μs, would typically take 180 ms to acquire. Successful EPI requires excellent B_0 homogeneity, T_2^*s on the order of 100 s of milliseconds and minimal magnetic susceptibility differences within the sample, which is not always possible. A major drawback with EPI techniques is that, because they are gradient echo techniques, the acquired signal is heavily weighted by T_2^* relaxation and the signal is therefore reduced *during* data acquisition. In conventional spin–echo imaging, any inherent relaxation weighting of the image is common to each of the individually acquired frequency encoded *k*-space lines. However, in EPI imaging each line in *k*-space will have a different T_2^* relaxation weighting. Far more important than just the reduction in signal that this gives are the image artifacts that this dephasing can cause. This means that in addition to T_2^* signal attenuation related problems, EPI also suffers from complications/drawbacks related to the fact that the effective bandwidth in the phase encode direction is severely limited (Mantle and Sederman, 2003). EPI in general is not suited for pharmaceutical research applications.

4.2. Low excitation angle imaging

Haase et al. (1986) have shown that a rapid two-dimensional image may be acquired based on a simple single gradient echo imaging sequence. As with traditional imaging sequences, a single gradient echo (and phase encode step) are acquired per r.f. excitation but here the repetition (recycle) time of the experiment is reduced to a few ms. Thus a 128×128 image based on a repetition time of 3 ms would take approximately 384 ms to acquire and is thus around a factor of two slower than EPI. The crux of this technique is that the r.f. excitations involve a low r.f. excitation flip angle (θ), typically 5–10°. This technique has been termed Fast Low Angle Shot imaging (FLASH) or SNAPSHOT imaging. The signal resulting from a small flip angle θ is proportional to $\sin\theta$, while the longitudinal magnetisation that remains after the excitation is proportional to $\cos\theta$. The net result is that it is possible to acquire rapidly successive lines in *k*-space to build up an image in a short time. FLASH images do not suffer from the same amount of T_2^* weighting that EPI does. Unlike the other fast imaging sequences presented so far, FLASH only uses a small fraction of the full magnetization per excitation (and hence each line in *k*-space) and therefore suffers from an inherently low signal-to-noise ratio as the amount of magnetisation transferred to the transverse plane is small. Repetitive reading of this magnetisation causes some further signal loss but this is partially compensated for by spin–lattice relaxation. Practically, small values for the ratio of the repetition time to the spin–lattice relaxation time are chosen to minimise the image acquisition time. The acquired magnetization, $M(t)$, is given by:

$$M(t) = M_0 \cos^n \theta \sin \theta \tag{1.14}$$

where M_0 is the equilibrium magnetization, θ is the excitation flip angle and n is the number of the excitations. Clearly, if θ is too large, there will be little magnetization left for high n but if θ is small, only a small proportion of M_0 is transferred to the transverse plane. For this reason the number of steps in the phase direction is often reduced from 128 to 32 or even 16 so that a greater θ can be used and thereby increasing the signal-to-noise ratio (SNR). The use of a homospoil gradient, usually incorporated as a prolonged readout gradient, at the end of the acquisition sequence is very important to remove interference between unwanted transverse coherences from previous excitations and the true signal. With FLASH imaging there is clearly a trade-off to be made between imaging speed and SNR/image resolution. The speed may be increased at the expense of image resolution or a greater repetition time, *TR*, allowing for more T_1 relaxation and therefore an improved SNR whilst decreasing imaging speed. Short *TR* FLASH is relatively insensitive to T_1 relaxation times since no species is allowed time for T_1 relaxation. In a similar way to EPI imaging, for FLASH imaging, each line acquired in *k*-space will have a different magnetization associated with it which will often affect image contrast. By altering the order in which the lines in *k*-space are acquired, the contrast may also be altered, most commonly achieved by using a centered *k*-space raster such that lines at the center of the *k*-space raster are acquired first to improve SNR though at the expense of image resolution. Unlike EPI imaging FLASH is reasonably insensitive to susceptibility and motion artifacts because of the short time for which the gradients are actually active, though sample inflow into the imaging slice can produce significant signal contrast. In terms of pharmaceutical research FLASH imaging is more attractive than EPI. Quantitative FLASH imaging requires that both T_1 and T_2^* relaxation contrast in the images be corrected for, which is possible by the acquisition of individual series (typically eight) of both T_1 and T_2^* weighted images. However, T_1 contrast is usually minimised by choosing a small enough excitation flip angle, typically between 2° and 5°, to make the image independent of T_1. To the author's best knowledge, there have been no publications of quantitative FLASH imaging techniques applied to pharmaceutical research in the literature, perhaps because of the low signal to noise ratio associated with FLASH.

4.3. Multiple spin–echo rapid acquisition with relaxation enhancement (RARE) imaging

The first practical implementation of multiple spin–echo imaging was first demonstrated by Hennig et al. (1986) who introduced Rapid Acquisition with Relaxation Enhancement (RARE) imaging. The general details of the multiple spin–echo imaging method and its effect upon image quantitation is discussed in more detail in

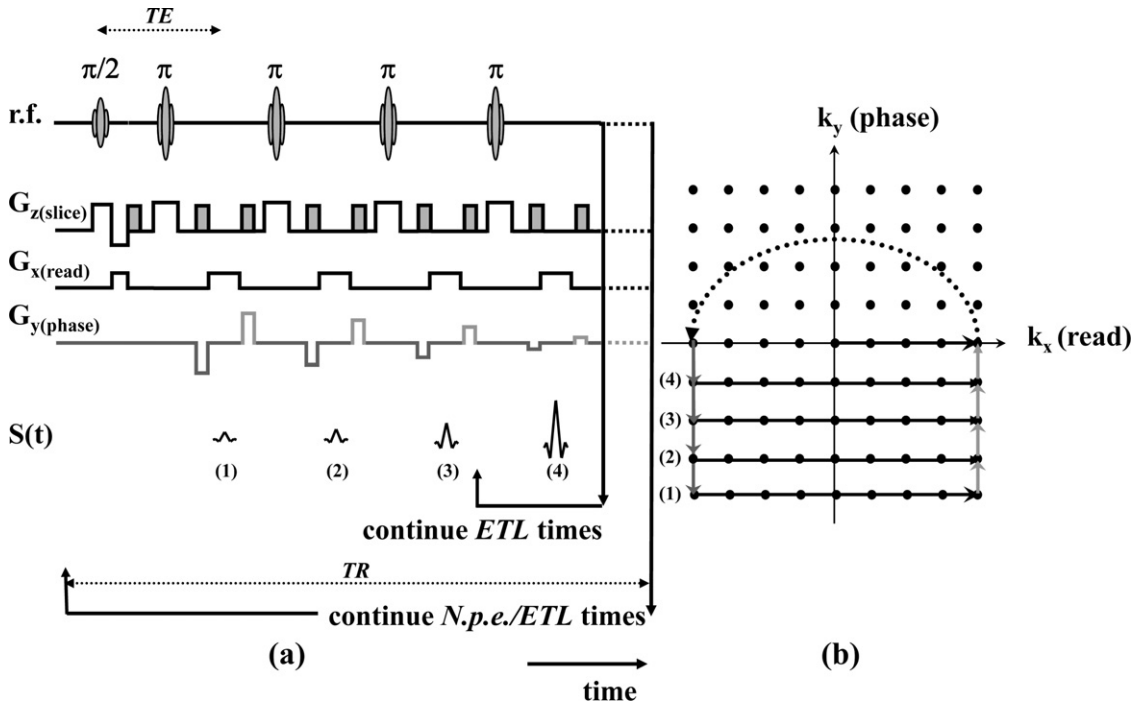

Fig. 6. *k*-space trajectory (b) of a RARE spin–echo imaging sequence (a). The order of the phase encoding is shown by the numbers to the left of the raster. After each line in *k*-space the spins are returned to the same point on the $k_{x\ (read)}$ axis prior to the application of the refocusing pulse shown by the dashed line and arrow. For RARE imaging the magnitude of the successive phase encoding gradients pairs is incremented in incremented throughout the echo train. The basic image acquisition time for a single scan RARE image is given by the product $(TE \times N.p.e) + TR \times (N.p.e/ETL - 1)$. *Note*: $ETL \leq N.p.e.$

Supplementary material section A.3. The multiple echo acquisition mode discussed in Section A.3 assumes that each successive readout echo had the same value for the phase encod step and thus the actual time taken to acquire a multiple-echo image is essentially equivalent to a conventional spin–echo imaging technique. In order to speed up the acquisition process of a single image, a series of α-degree refocusing r.f. pulses (typically with α approaching π) are used to acquire multiple *k*-space lines for a single r.f. excitation pulse, but the major difference being that each successive frequency encoded readout echo has a different value for the phase encoding step as shown in Fig. 6. In this case the total image acquisition time for a single scan is given by the product $(TE \times ETL)$, where *ETL* is the echo train length.

This type of image acquisition was first realised by Hennig et al. (1986) and was termed RARE imaging or Rapid Acquisition with Relaxation Enhancement imaging. This pulse sequence and its variants, (turbo spin–echo (TSE) and fast spin–echo (FSE)) are similar to modern, i.e. blipped, EPI pulse sequences in that after acquisition of a single line in *k*-space the coherent signal is refocused and used to acquire further lines in *k*-space. A typical single excitation 128 × 128 RARE image with a 512 μs Gaussian soft refocusing pulse (with the same acquisition bandwidth as the EPI discussed previously) and an *ETL* = 128 would take around 360 ms to acquire and is thus similar to FLASH, and approximately twice as long as EPI imaging, in terms of total image acquisition time. Two major differences between traditional EPI and RARE are:

In RARE imaging every readout gradient sequence is interrupted by an α degree selective r.f. refocusing pulse.

At the end of the each RARE readout sequence, a phase unwinding gradient returns the magnetisation to the same place in the *k*-space, before each α r.f. refocusing pulse.

Despite the drawbacks associated with multiple-spin echo methods (described in Supplementary materials section A.3) quantitative spin–density, T_2 relaxation and self-diffusion coefficient RARE imaging is possible and was first introduced by Norris et al. (1992) who showed that pre-conditioning the basic RARE imaging sequence with either inversion recovery relaxation weighting (T_1), Hahn echo relaxation weighting (T_2) or a standard stimulated echo diffusion weighting, allowed spin-density and self-diffusion coefficient images to be calculated. Sederman et al. (2003) have shown that for systems where $T_1 \approx T_2$ (usually liquids) multiple RARE images from a single excitation can be used to extract quantitative spin–density and T_2 images to less than 10% error. Chen et al. (2010) have recently shown it is possible to obtain quantitative water ^{1}H spin density RARE images in less than 2 min. Chen et al. (2002) also showed that the 13-interval APSGTE diffusion preconditioning of a stanard RARE sequence also gave quantitative maps of water self-diffusion coefficient in less than 2 min for a water phantom. The use of the 13-interval Cotts et al. (1989) magnetisation preconditioning as opposed to traditional stimulated-echo diffusion magnetisation preconditioning has the advantage that signal losses due to diffusive attenuation in background magnetic field gradients is minimised. Background magnetic field gradients are likely to be present in all but the simplest of samples (i.e. pure liquids) and thus must be minimised for quantitative analysis. Chen et al. (2010) found that optimal quantitative CPMG-T_2 and diffusion preconditioned images for a single shot 64 × 64 data matrix were obtained for a RARE phase encoding start value (Norris et al., 1992) (*PESV*) of −0.2. The reason for changing the value of the *PESV* is that standard RARE imaging is usually performed with a *PESV* equal to +/−1 which means that the phase encoding order of the echo train starts from the most negative (or positive) value, i.e. the 'edge', of *k*-space first and then linearly increases (or decreases) its value, through zero to the most positive (or negative) value of *k*-space. It is well known (Callaghan, 1993; Haacke, 1999) that the absolute spin density of a sample is proportional to the signal acquired at the center of *k*-space, i.e. when the phase encoding gradient is zero; however the *quality* of the resulting RARE image in terms of spatial resolution is determined by the edges of *k*-space, i.e. those acquired with the maximum value of the phase encoding gradient. So, whilst

standard RARE imaging with $PESV = -1.0$ gives a good overall quality image resolution wise, it may suffer from adverse T_1/T_2 contrast (especially when $T_2 \ll T_1$) and hence a poorer signal-to-noise ratio, because of the time that elapses from the initial excitation pulse to the acquisition of the *center* of *k*-space[2] is relatively long in a standard linear phase encoding scheme. For example the center of *k*-space for a 64×64 single shot linearly phase encoded RARE image with a $PESV = -1.0$ with a primary echo time $TE = 2.5$ ms will be acquired with an effective echo time, TE_{eff}, for a standard linear phase encoding scheme given by:

$$TE_{eff} = TE + TE\left\{\left(\frac{ETL}{2} - 1\right) \times \left|PESV\right|\right\} \tag{1.15}$$

and is approximately equal to 80.0 ms for the parameters given here. Thus, in such a sequence, any molecular species having a T_2 less than 80.0 ms will experience at least a 64% attenuation before the actual signal is acquired. Why then, do standard RARE imaging sequences supplied with a spectrometer not start with a $PESV = 0$ where $TE_{\text{eff}} = TE = 2.5$ ms in order to minimise relaxation losses and hence maximize quantitative information? The quick answer is that it does in terms of absolute spin density, but this comes at the price of image resolution/definition. For $PESV = 0$ the first (non-phase encoded) pure T_2 weighted spin–echo of the echo train corresponds to the center of *k*-space and thus any T_2 relaxation artifacts in the image are minimised. The problem with this type of RARE acquisition mode, also known as centered[3] encoding, is twofold: (1) for nominally 180 degree refocusing pulses the phase encoding of the next few (by few we mean between six to eight) echoes will be severely affected by the oscillatory behaviour of the magnetisation (Hennig, 1988, 1991; Hennig et al., 2003, 2004; Leroux and Hinks, 1993; Norris and Bornert, 1993; Schick, 1997; Zur, 2004) as a consequence of the production of spin and stimulated echoes – (see Supplementary materials section A.3) leading to severe artifacts in the final image; (2) centered linear phase encoding results in the edges of *k*-space ($\pm k_y max$) being encoded at approximately $(TE + TE \times (ETL - 1)/2)$ longer in time from the initial excitation pulse than for PESV = −1.0 and thus the image will suffer from a loss of spatial resolution/definition in the phase encode direction which results in blurring or smearing of the image. For completeness we should mention that *centric* encoding whilst giving a good signal-to-noise ratio (and minimised T_2 contrast) in the final image (see footnote 3) results in an even greater loss of image definition/resolution in the phase encoding direction than centered phase encoding as the edges of *k*-space are acquired right at the end of the echo train, i.e. at a time defined by $(TE \times ETL)$. As Eq. (1.15) indicates, optimising the value of the *PESV* of a standard RARE sequence depends upon the *ETL*, the flip angle of the refocusing pulse, the type of soft excitation pulse used and the performance of the radio frequency coil, and thus specific advice to the experimenter is extremely difficult to give here; however some guidelines are given at the end of Section 4.4.

4.3.1. Diffusion weighting in multiple spin–echo imaging

An exact analytical expression for the diffusion weighting of read, phase, slice and homospoiling gradients in a multiple-echo imaging sequence is dependent upon the actual pulse sequence used. However, the expressions described by Brandl and Haase (Brandl and Haase, 1994) in section [A.2] for a simple gradient/spin–echo sequence may be adapted, with some algebra, to give approximations of diffusion losses in multiple-echo imaging sequences. In essence one needs to inspect a pulse sequence, identify the symmetry of the various magnetic field gradients, their magnitudes (which may vary as in the case of phases encoding gradients) and their timings about the 180° refocusing pulse and then use this as a starting point to formulate an expression, for each individual orthogonal gradient direction. The resulting expression will be the product of a series of exponentials which will then reduce to a single exponential whose exponent involves both gradient time and gradient strength dependent functions of the general form:

$$I(TE_n) = \exp\left(-\gamma^2 D \sum_{i=1}^{n} \partial_i{}^2 g_i(n)^2 \left(\Delta - \frac{\delta_i}{3}\right)\right) \tag{1.16}$$

where n is the *ETL*, $g_i(n)$ reflects the fact that the gradient magnitude may change as n increases. For standard RARE multiple-echo imaging sequences the read, slice and spoiler gradient strength will be fixed, but the phase encoding gradients will vary with n.

4.4. Single point imaging

Whilst the method of single point imaging (SPI) (previously referred to as Constant Time Imaging, (CTI)) has been known (Emid and Creyghton, 1985; Gravina and Cory, 1994) to the NMR community since the mid 1980s it has only recently been applied to pharmaceutical research. The key difference between single point imaging and conventional spin–echo imaging is that SPI acquires only one point of *k*-space for every r.f. excitation pulse. SPI is a pure phase encoded technique, i.e. a magnetic field gradient is switched on, and after a suitable gradient stabilization time has elapsed, a short intense r.f. pulse is applied. Following this r.f. pulse a phase encoding time is allowed to elapse which is typically anywhere between 20 and 300 μs. Fig. 7 shows a typical three dimensional single point imaging pulse sequence.

The SPI technique is used to image samples where the molecular species are either solid or immobile and thus such species have extremely short $T_2{}^*$ values. Therefore, SPI requires that a *k*-space data point is sampled as soon as possible after the r.f. excitation pulse, which in turn ensures that the acquired data point has only a relatively small amount of $T_2{}^*$ weighting. The disadvantage of SPI imaging and related techniques is that it can be extremely time consuming when three dimensional spatial information is required (two dimensional SPI is not usually possible[4]). The long acquisition time of 3D SPI imaging is due to the fact that every single *k*-space point must be acquired individually from successive r.f. excitation pulses. To reduce the 3D SPI imaging time to manageable quantities low angle r.f. excitation pulses are used in a similar fashion to FLASH imaging and thus whilst a quicker image may be acquired, the signal-to-noise ratio consequently suffers. A single scan $64 \times 64 \times 64$ data matrix 3D single point image, employing a 5° r.f. excitation tip angle a recycle delay of 10 ms would take approximately 0.7 h which, realistically, would double as two signal averages would usually be required. One dimensional SPI is thus a more feasible option in terms of image acquisition times and it is obvious that a good quality single point 1D image profile can be acquired in well under a minute. However, for one dimensional SPI one must appreciate that information is lost in the orthogonal plane

[2] In multi-echo MRI the time that elapses from the initial magnetisation excitation pulse to the acquisition of the echo at the center of *k*-space, i.e. when the phase encoding gradient is zero, is also known as the effective echo time, TE_{eff}.

[3] Note that "centered" and "centric" phase encoding terminology can have two different meanings. *Centered* in this work refers to a linearly incremented phase encoding scheme starting from 0, i.e. 0, $+0.1 \times k_y$max, $\rightarrow +1.0 \times k_y$max, $-1.0 \times k_y$max, $\rightarrow -1.0 \times k_y$max. *Centric* encoding is generally associated with the acquisition of successive alternating positive and negative values of the phase encoding step starting from 0, i.e. 0, $\pm 0.1 \times k_y$max, $\pm 0.2 \times k_y$max$\rightarrow \pm\ 1.0 \times k_y$max.

[4] 2D slice selective SPI using soft r.f. excitation pulses would be futile as the magnitude of the phase encoding gradient, during which the soft r.f. excitation would be applied, changes with every excitation step and thus the slice thickness would change accordingly, making the data meaningless.

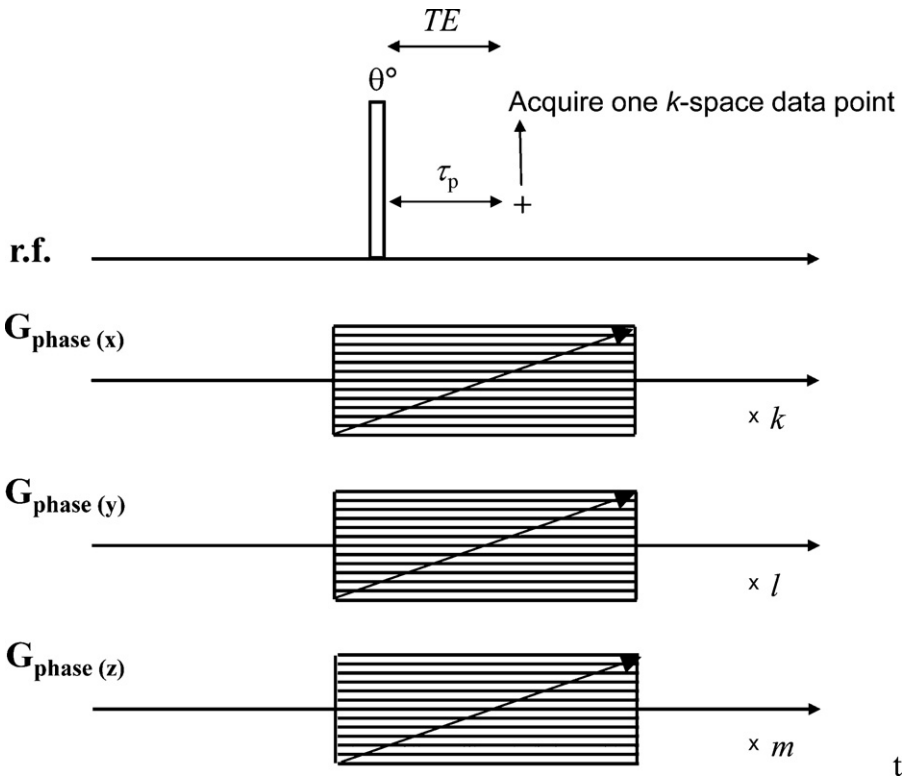

Fig. 7. Schematic showing the 3D single point imaging sequence. Following an excitation pulse (during the application of the gradients) the system is allowed to evolve for a short phase encoding delay t_p. A single data point '+' is then acquired and the whole sequence is repeated $k \times l \times m$ times where k, l and m are the data matrix size for each orthogonal Cartesian direction.

and may lead to ambiguous interpretation of the data. A significant limitation of the 3D SPI technique and its application to micro-imaging is because the magnetic field gradient strengths required for high resolution spatial encoding on commercial MRI systems are simply not yet attainable. For example, a 128 data point (N_{pix})1D SPI profile taken over say a 5.0 mm field-of-view (FOV), giving a spatial pixel resolution of 39 μm, with a phase encode time, $\tau_p = 100$ μs would require a maximum gradient strength, G_{max} given by Eq. (1.17), viz:

$$\mathbf{G}_{\max} = \frac{2\pi}{\gamma\tau_{\mathbf{p}}}\frac{\mathbf{N}_{pix}}{\mathbf{FOV}} \tag{1.17}$$

For the parameters given above Eq. (1.17) gives a maximum gradient strength of approximately 600 G cm^{-1} which is way beyond the capabilities of any current commercially available 3-axis gradient system. Of course, Eq. (1.17) shows that the maximum gradient strength could be reduced by either increasing the phase encode time (at the expense of signal loss) or decreasing the spatial resolution. Clearly a balance between both has to be met!

In line with the conclusions of Section 3.1, some practical guidelines are given below with regard to the use of fast magnetic resonance imaging sequences in pharmaceutical research.

Avoid EPI imaging if possible! Good quality, quantitative, sub-millimeter spatial resolution EPI images require the T_2* relaxation time within each pixel of the image to be on the order of 100 of ms (which is equivalent to a full width at half maximum linewidth of NMR spectrum of the bulk system equal to approximately 3 Hz!), which is extremely unlikely for many pharmaceutical tablet research systems.

FLASH imaging may be used as a much more robust alternative to EPI imaging. The benefits of FLASH are: it is relatively insensitive to T_1 weighting, provided a low enough flip angle is chosen; although it is T_2* weighted, T_2* contrast is minimised by the use of short echo times (typically 1–2 ms), and the T_2* weighting can be characterised and by acquiring several FLASH T_2* weighted images; FLASH is relatively insensitive to motion artifacts, again due to the very short echo-times associated with FLASH imaging and may thus be appropriate for flowing dissolution media research; FLASH imaging may also be preferred for continuously changing systems, as once the flip angle has been optimised then the sequence can be repeated every few milli-seconds without the need to wait for a long time between successive excitations. It must be stressed that gradient spoiling (Haacke, 1999) at the end of the readout period in a FLASH experiment is essential for artifact free images. In addition r.f. pulse (Haacke, 1999) spoiling may also be used to eliminate unwanted signals.

RARE imaging is robust fast spin–echo based technique that may be preferred over FLASH when $T_2^* < T_{2eff}$ as the immediate benefit is a large increase in signal-to-noise ratio merely from the fact that a 90° excitation pulse is used in RARE as opposed to a 5° excitation pulse in FLASH (see Eq. (1.14)). If quantitative RARE imaging is required then it essential that the primary echo time, TE, is minimised so that the effective echo time TE_{eff} is also minimised. In addition, nominally 180° soft refocusing pulses[5] should be used as opposed to smaller flip angle pulses to minimise the stimulated echo pathway and hence minimise the T_1 relaxation weighting in the echo train. Depending upon the system under investigation, the data matrix resolution required, and whether the absolute spin density or image definition takes priority, for a standard (sequential) linear phase encoding scheme (including centered encoding) it

[5] Nominally 180° refocusing flip angles are generally not used in a clinical environment due to excessive r.f. power dissipation to the patient.

may be advantageous to alter the PESV anywhere between −1.0 and −0.0 to obtain optimal images. Standard[6] *centered* or *centric* encoding is not recommended (Chen, 2010) due to the cumulative image quality reduction resulting from echo oscillations and excessive image blurring due to the edges of *k*-space being poorly resolved. Signal losses due to diffusion in high spatial resolution (typically less than 100 μm) RARE experiments should be considered using the approach.

For commercially available micro-imaging spectrometers (which includes both high field superconducting systems and bench-top systems), SPI micro-imaging is likely only to be useful for one-dimensional image profiling at a rather low resolution, (c.a. > 200 μm) because of the limitations associated with available gradient strength, signal-to-noise ratio, and, for 3D spatial imaging, total signal acquisition time.

5. Quantitative magnetic resonance imaging in pharmaceutically relevant research

In the last twenty years there have been many NMR and MRI research papers that have focused on studying both non-swelling and swelling matrix type controlled / sustained drug delivery dosage forms. Section 1.0 indicated that several recent reviews (Melia et al., 1998; Nott, 2010; Richardson et al., 2005; Zeitler and Gladden, 2009) essentially cover most of these works to date. The aim of this section is to review the literature that is concerned primarily with *quantitative* MRI studies of pharmaceutically relevant research. Again it is stressed that *quantitative* in this context means, how much? (species spin-density), how fast? (self-diffusion, transport diffusion and flow) and where (spatial location)? This section is sub-divided into three main areas: (1) the applications of quantitative MRI to non-swelling drug delivery devices; (2) the application of quantitative MRI to swellable delivery devices, i.e. hydrogels; (3) the applications of quantitative MRI to study matrix dissolution phenomena.

5.1. Quantitative MRI of non- swelling polymeric systems

Hyde et al. (1995a) presented the first quantitative magnetic resonance study of the diffusion of decalin into ultra-high molecular weight polyethylene (UHMWPE). Whilst UHMWPE is not of direct pharmaceutical relevance Hyde et al. showed the methodology by which quantitative ^{1}H solvent profiles could be obtained from data despite the influence of both T_1 and T_2 contrast effects. T_1 and T_2 maps were obtained at a point in the uptake of liquid where the greatest range in liquid concentration was observed. The intensity of signal corresponding to liquid in the polymer was compared to that of pure liquid in a reference sample, and correlations for T_1 and T_2 values versus signal intensity were used to deconvolve relaxation contrast, to yield the true liquid concentration. The technique was used to study the effect of the degree of crosslinking of UHMWPE, on the swelling kinetics and decalin transport within the polymer. A single Hahn spin–echo imaging technique was used with a recycle delay approximately equal to the average spin–lattice relaxation time of the liquid, and an echo time approximately half the average spin–spin relaxation time. Under these conditions the relaxation contrast was significant, yet the mass uptake data derived from the concentration profiles obtained, using the method of analysis described, agreed well with gravimetric data. In a similar study Hyde et al. (1995b) examine the effect of incorporating a high molecular weight peptide in biologically relevant 50:50 poly(glycolide-co-DL-lactide) using a multiple slice Hahn spin–echo imaging technique. Hyde et al. (1995b) showed it was possible to qualitatively and quantitatively probe the effect of the presence of drug on the buffer uptake kinetics, the polymer morphology, the physico-chemical environment of the liquid in the polymer, and the drug distribution within the polymer. Rapid Super-Case II buffer diffusion was observed in the drug-free polymer, while much slower diffusion was observed in the drug-loaded material, approaching Fickian and Case II limits in different regions of the polymer. A strong drug–polymer interaction was observed which affected the polymer chain configuration and mobility, and therefore the transport of buffer molecules in the polymer.

Harding et al. (2000) used both diffusion weighted NMR spectroscopy, multi-slice spin–echo imaging and quantitative three-dimensional imaging magnetic resonance techniques to study the drug release process from small (sub-mm) lipophilic matrix theophylline beads. NMR microscopy was used to follow the ingress of the dissolution medium into the beads. Pulsed gradient spin–echo (PGSE) NMR and 3D MRI were used to measure the mobility and distribution of liquid within fully liquid penetrated beads. Fig. 8 shows images of selected two-dimensional slices taken from the T_1/T_2 relaxation corrected data sets which show the true spin density along with the T_1 and T_2 relaxation maps.

These techniques were used to rationalise the increase in the drug release rate with increasing proportion of GMS (glycomonosaccharide):paraffin in the matrix composition. A well-defined penetrant front was seen to move towards the center of the bead during the dissolution process and the rate of liquid uptake showed the same trend with increasing GMS content as the rate of drug release. The total concentration of absorbed liquid was observed to increase and its T_2 relaxation time decreased with increasing GMS content of the bead matrix. This, combined with the interpretation of PGSE results suggested that liquid resided in the matrix material as well as in pores left by the dissolved drug, and that this tendency increased with increasing GMS content. Heterogeneities in liquid distribution within the beads were also quantified using percolation analysis and were related to the lipid matrix composition which was thought to be a possible contributory factor in determining the rate of drug release.

Djemai et al. (2001) used standard quantitative T_2-weighted single spin–echo MRI to investigate the degradation of drug-loaded poly(glycolic lactic acid) (PGLA) 50:50 cylinders. Spatial variations in the rate of degradation throughout the polymer cross-section were observed non-invasively via quantitative imaging of penetrant concentration, T_2 and self-diffusion coefficient. This spatial variation in the rate of degradation was attributed to the quicker degradation in the inner region of the sample due to the autocatalytic cleavage of polymer ester bonds by carboxyl end groups which were generated by ester bond cleavage.

Chowdhury et al. (2004) use a three dimensional T_2-relaxation weighted spin–echo MRI protocol to quantify the absolute water concentration and dynamic transport diffusive ingress of water into poly(2-hydroxyethyl methacrylate), PHEMA, loaded with either one of two model drugs, vitamin B12 or aspirin, at 37 °C. The PHEMA was loaded with 5 and 10 wt% of the drugs. Fig. 9 shows two typical images extracted from the three dimensional data for the water protons that had diffused into a PEHMA cylinder containing 10% weight aspirin after water sorption at 37 °C for (a) 6.3 h and (b) 18.1 h.

One dimensional profiles were extracted from the three dimensional images and it was observed that incorporation of vitamin B12 into PHEMA resulted in enhanced crack formation on sorption of water and the crack healing behind the diffusion front was slower

[6] There are a number of non-standard ways available in the literature to alleviate the problems associated with image artefact from echo oscillations and thus make centered and centric RARE imaging more attractive. However these are rarely if at all implemented with commercial spectrometers and require specialist knowledge. The interested reader is urged to consult the work of Hennig, Le Roux and Zur for a detailed analysis (see references for details).

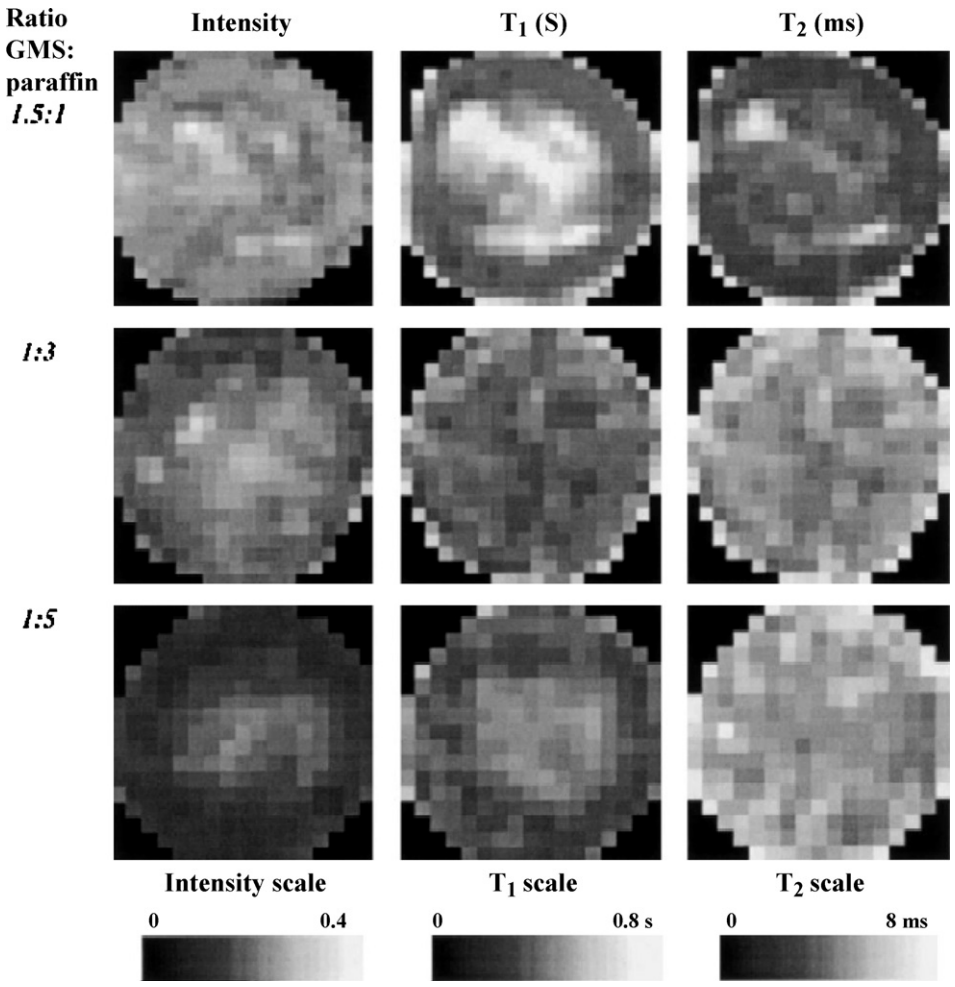

Fig. 8. Selected 2D slices from 3D images of fully liquid saturated beads. The images show signal intensity (after corrections for relaxation contrast) and liquid T_1 and T_2 relaxation times for beads with GMS:paraffin ratios of 1.5:1, 1:3 and 1:5. Reproduced with permission from reference (Harding et al., 2000).

than for PHEMA without added drug. This was accounted for by the anti-plasticization of PHEMA by vitamin B12. Crack formation was inhibited in the PHEMA-aspirin systems because of the plasticizing effect of the aspirin on the PHEMA matrix. All of the polymers were found to absorb water according to an underlying Fickian diffusion mechanism. For PHEMA loaded with 5 wt % of aspirin or vitamin B12, the optimal values of the water diffusion coefficients were both found to be $1.3 \pm 0.1 \times 10^{-11}\ m^2\ s^{-1}$ at 37 °C, while the values for the polymer loaded with 10 wt% of the drugs were slightly higher at $1.5 \pm 0.1 \times 10^{-11}\ m^2\ s^{-1}$.

Djemai and Sinka (2006) described the use of ^{1}H MRI for 3D mapping of the relative density distribution in pharmaceutical tablets manufactured under controlled conditions. The tablets were impregnated with a compatible liquid which acted as an inert probe molecule for interrogation using the MRI technique. Their technique involved imaging the presence of liquid which occupied the

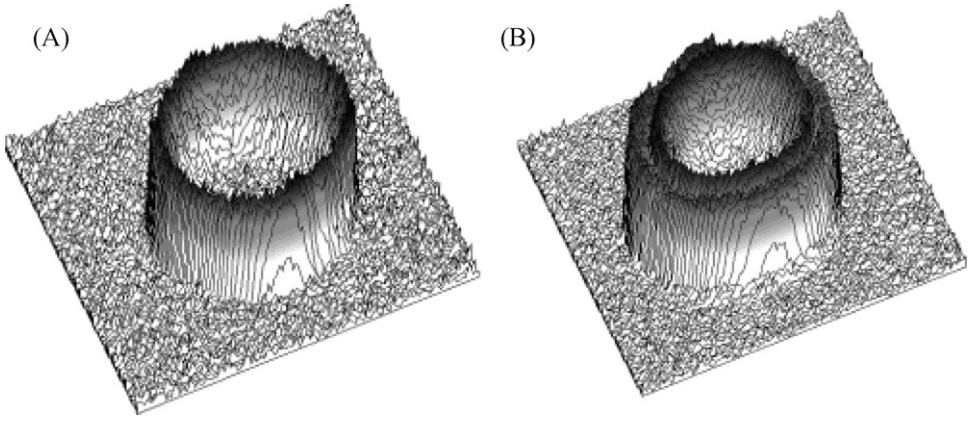

Fig. 9. MRI of the water protons in a PHEMA cylinder containing 10 wt % aspirin after water sorption at 37 °C for (A) 6.3 h and (B)18.1 h. The double layer visible in (B) is due to crack formation. Reproduced with permission from reference (Chowdhury et al., 2004).

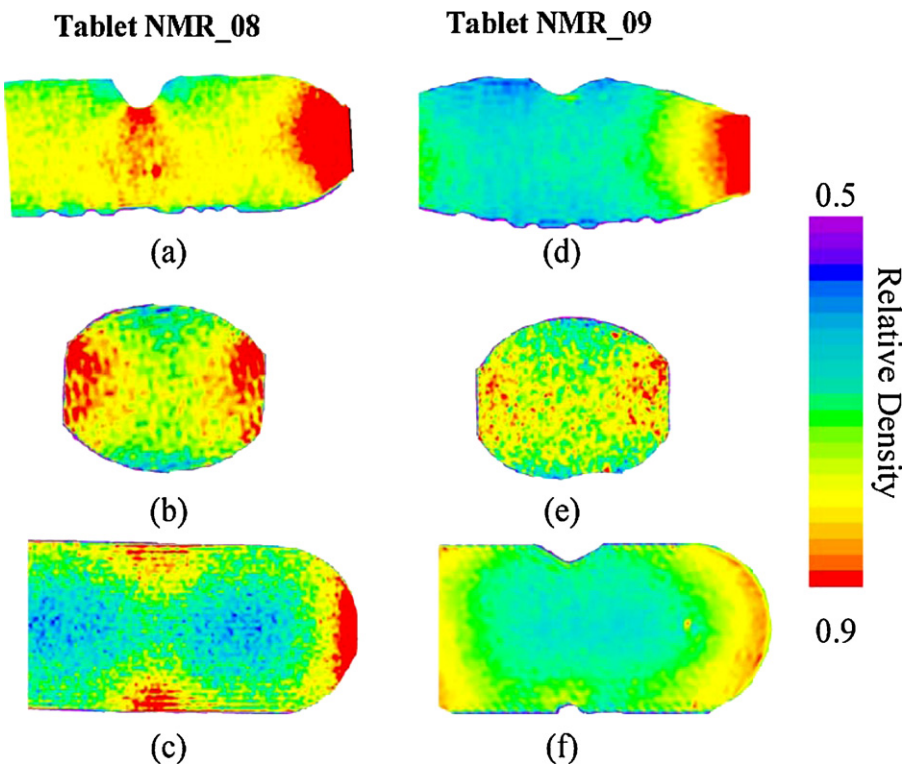

Fig. 10. Relative density maps in *Y–Z* cross-sections (a and d), *X–Y* cross-sections (b and e), and *X–Z* cross-sections (c and f). Reproduced with permission from reference (Djemai and Sinka, 2006).

open pore space. The method did not require special calibration as the signal was directly proportional to the porosity for the imaging conditions used. The MRI method was validated using uniform density flat faced tablets and also by direct comparison with X-ray computed tomography. Fig. 10 shows an example of the experimental MRI results of Djemai and Sinka (2006) for capsule shaped tablets.

The collective results reported by Djemai and Sinka (2006) showed that their MRI method highlighted: (1) the effect of die wall friction on density distribution by compressing round, curved faced tablets using clean and pre-lubricated tooling; (2) the evolution of density distribution during compaction for both clean and pre-lubricated die wall conditions, by imaging tablets compressed to different compaction forces; and (3) the effect of tablet density distribution on the image by compressing two complex shaped tablets in identical dies to the same average density using punches with different geometries.

Karakosta and McDonald (2007) used 2D spin–echo MRI to map the dynamic ingress of water into a nominally non-swelling polymer matrix slow-release drug delivery device comprising a compact of Eudragit polymer and Diltiazem hydrochloride drug. Quantitative analysis of the diffusion fronts showed that the water ingressed with the square root of time and thus it was concluded that the ingress behaviour was Fickian like and that the drug release was weakly dependent on the drug particle size. A dissolution-diffusion model, based on Fick's laws and the Noyes–Whitney equation, which specifically incorporated the drug particulate size was developed and showed good agreement with the experimental data. Karakosta and McDonald (2007) also showed, theoretically, that the drug release should become Fickian like and particle size dependent as long as the drug dissolution constant was reduced substantially.

Collins et al. (2007) used a combination of quantitative ^{1}H CPMG T_2-relaxation and PFG-NMR diffusion studies with spin–echo imaging to examine the evolution of the internal pore structure of partially soluble pharmaceutical pellets as they absorbed water and released soluble components. The restricted diffusivity of water trapped within the pellets was measured by PFG-NMR and the data from this was subsequently used to calculate the surface-to-volume ratio and tortuosity of the pore structure, which enabled an unambiguous assignment of the pores size distribution. The data was analysed using a combination of mathematical regularisation and the Brownstein–Tarr model to give pore size distributions.

Fig. 11 shows the temporal evolution of the calculated pore size distributions, assuming spherical pores, for both drug loaded and placebo pellets. It was clear that pore size distribution for both formulations changed with time; the drug loaded pellets showed a relatively narrow PSD at short immersion times which broadened as the immersion time increased. The placebo pellets showed a noticeable bimodal pore size distribution at short immersion times which gradually disappeared for longer immersion times. Spin–echo imaging techniques were also used to help explain the observed behaviour of the pore size evolution for drug-loaded and placebo pellets. Fig. 12 shows four sets of images that illustrated the different water uptake mechanisms of the drug-loaded and placebo pellets; the water uptake for the drug loaded pellets was homogenous and occurred rapidly, whilst the placebo pellets showed greater evidence for a water diffusion front.

5.2. Quantitative MRI of swelling polymeric matrices: hydrogels

Some of the first research yielding quantitative transport diffusion coefficients from MR imaging was that of Ashraf et al. (1994) who analysed single spin–echo images to extract the water penetration rates and hence calculate the transport diffusion coefficient in a hydrophilic polymer matrix capsule consisting of pseudoephedine HCl and hydroxypropyl cellulose (HPC). The water penetration rate was determined according to the imaging intensity difference between the dry and wet areas in the cross-sectional

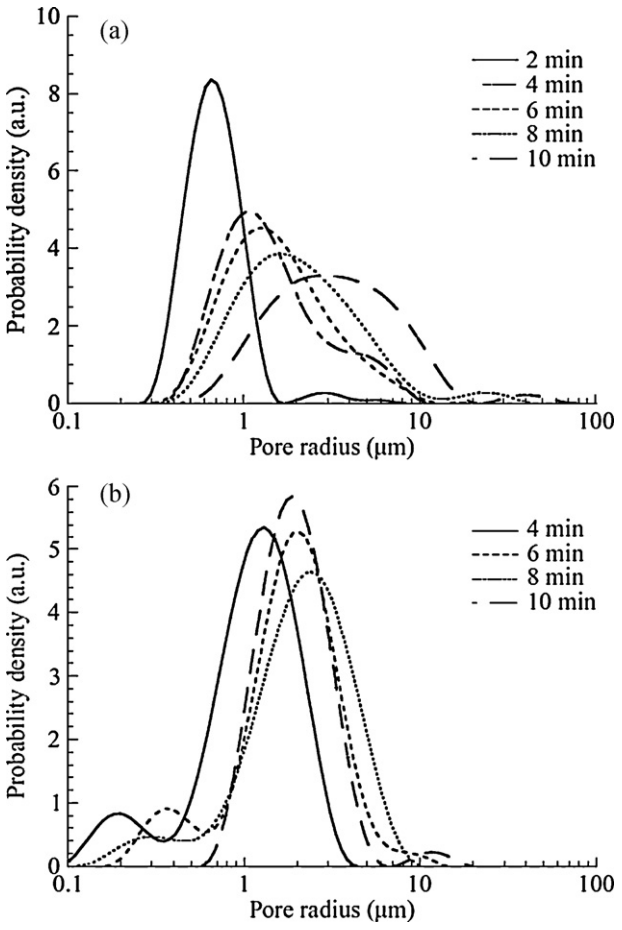

Fig. 11. Calculated pore size distributions at different immersion times for a drug-loaded pellet (a) and placebo pellet (b). Reproduced with permission from reference (Collins et al., 2007).

slices of the sample at different time points; a water transport diffusion coefficient in the gel of 4.15×10^{-10} m^2 s^{-1} was calculated by applying the Jost equation (Pitkin and Carstens, 1973) as given by Eq. (1.18):

$$\ln(m) = -\left(\frac{D\pi}{r_0^2}t\right) \tag{1.18}$$

where r_0 was the radius of an equivalent sphere and m represented the percentage dry core of the original size of the tablet, and D was the transport diffusion coefficient of water.

Bowtell et al. (1994) used diffusion weighted and T_2-relaxation weighted spin–echo MRI techniques to monitor the formation of the gel layer in a hydrating drug loaded HPMC tablet in distilled water under 37 °C. The axial image of a swollen tablet showed that the tablet developed a concave shape (convex in the radial image) which was postulated to be caused from a higher rate of hydration at the edges of the tablet, giving rise to greater expansion, as the stress in these regions of the matrix was more rapidly released. The T_2 value of water in the gel layer was found to vary between 90 and 30 ms whilst the diffusion coefficient was found to vary from 2.2×10^{-9} to 1.3×10^{-9} m^2 s^{-1}. The MRI technique was also found to be useful in identifying the distribution of insoluble drug particles within the gel coat of the hydrating tablet.

Gao and Fagerness (1995) determined the diffusivities of drug (adinazolam) and water in HPMC gel samples by 1D pulsed field gradient spin–echo (PFG-SE), according to Stejskal-Tanner equation (Stejskal and Tanner, 1965). They found that drug diffusivities in a non-interactive multi-component system showed an exponential dependence upon the concentration of the viscosity-inducing agent (VIA) (glucose, lactose, maltoheptaose, and HPMC) and the degree of polymerization of the VIA. However, this behaviour was found to be independent of the nature of the polymer viscosity grades.

Rajabisiahboomi et al. (1994) used a 2D MRI imaging technique (the exact sequence was not specified) to investigate the structure change of the placebo HPMC matrix during hydration in water at 37 °C. They claimed that the hydration at the edge of the tablet was much greater than that in the center, and this uneven swelling resulted in a convex shaped hydration layer during the early stages of water uptake. They also found that the rate and extent of gel growth were similar in both radial and axial directions, whereas the core dimension shrank in the radial direction and expanded in the axial direction. In similar work Rajabi-Siahboomi et al. (1996) used a T_2 weighted Hahn echo imaging sequence, and diffusion weighted Hahn spin–echo method to measure the T_2 relaxation time constant and self-diffusion coefficient of water diffusing into a placebo HPMC polymer. A spatial gradient of both T_2 and self-diffusion coefficient (SDC) across the gel layer was found which indicated that there was a water mobility gradient across the gel layer of the HPMC tablet.

As first noted by Fyfe and Blazek (1997) a large portion of the MR studies in the literature on hydrogel drug delivery dosage forms were qualitative because the images were not acquired with parameters that guaranteed that the signal intensities throughout the images were not directly related to water concentration and only the behaviour of the water and not the polymer itself was investigated. Fyfe and Blazek (1997) were the first to study quantitatively a series of gel samples with known HPMC concentrations as external references to calibrate the relationship between T_1, T_2, the molecular self-diffusion coefficient (SDC), the image intensity, and the water/polymer concentration. Fyfe and Blazek (1997) used these references and 1D spin–echo ^{1}H MR profiles to reveal the polymer concentration profile as a function of distance and time across the HPMC compacts. They found that a swelling HPMC matrix consists of three regions: (1) an outer most region (containing less than 10% HPMC; (2) a gel layer (containing between 10% and 30% HPMC); (3) an innermost layer (more than 30% HPMC) where the polymer appeared to be solid-like. In a subsequent study, Fyfe and Blazek-Welsh (2000) used a similar calibration approach along with one dimensional ^{1}H and ^{19}F imaging methods to quantitatively study the release behaviour of two model drugs, triflupromazine–HCL and 5-fluorouracil (whose molecular weight is three times smaller than triflupromazine–HCL) from swelling HPMC tablets. It was found that triflupromazine–HCL was only released at the eroding edge of the tablet where the HPMC concentration was below 10%, whilst 5-fluorouracil was found to release much more rapidly from the HPMC tablet and appeared to escape by diffusion from regions as high as 30% HPMC. Fyfe and Blazek-Welsh concluded that a comparison of 'diffusion' properties could be useful in predicting the mechanism of drug release from other swelling hydrophilic matrix systems.

Hyde and Gladden (1998) used a one-dimensional, slice-selective magnetic resonance imaging technique to image in situ the penetration of water into biorelevent poly(ethylene oxide) (PEO). Spin–lattice relaxation time (T_1)-weighted imaging experiments provided simultaneous, quantitative measurements of polymer and water concentration profiles, penetrant front motion kinetics and swelling kinetics. The propagation of the penetrant front was observed to be a diffusion-controlled process, with no volume change on mixing during swelling. Excellent agreement was observed when comparing the polymer concentration profiles obtained from the T_1 analysis with those measured by ^{1}H imaging of PEO during penetration by D_2O, under which conditions only the polymer response was imaged. Hyde and Gladden (1998) found

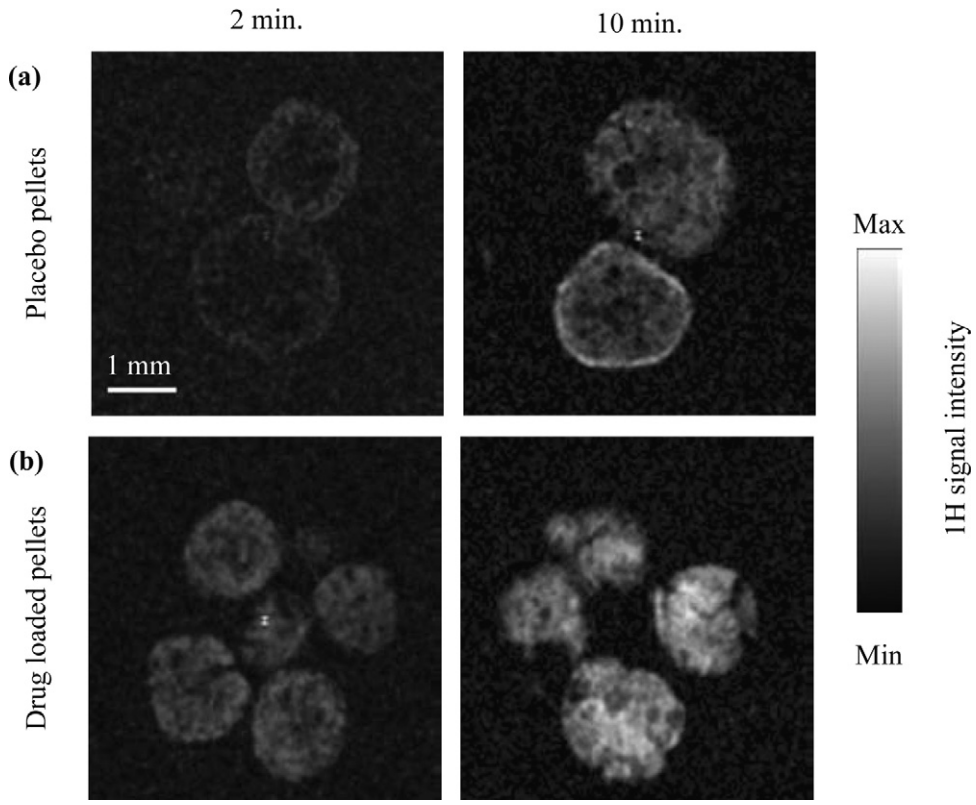

Fig. 12. Standard spin–echo images of placebo (a) and drug-loaded pellets (b) after they have been immersed for 2 min. (left) and 10 min. (right). The maximum intensity corresponds to PBS (phosphate buffer solution) signal intensity, which is approximately proportional to water content within the pellet. Reproduced with permission from reference (Collins et al., 2007).

that T_2 contrast was found to be negligible in their system and the data required no corrections for this.

Madhu et al. (1998) used T_2 weighted spin–echo and stimulated echo diffusion weighting imaging methods to study the dynamics and diffusion of the internal water flow in erodible hydroxypropylmethylcellulose (HPMC) and polyvinylalcohol (PVA) polymers. The polymers, in the form of tablets, were hydrated at 37 °C continuously and were monitored at regular intervals with a 500 MHz NMR microscope. The diffusion and spin–spin relaxation time (T_2)-weighted images revealed that the gel layer was strongly attached to the core of the tablet in both HPMC and PVA polymers. The spatial distribution of the water molecular self-diffusion coefficients and the T_2 relaxation times of the hydrating polymers were calculated from NMR microscopic images.

Tritt-Goc and Pislewski (2002) studied the transport behaviour of water in placebo HPMC tablets at two different pH values using proton imaging and T_2 maps derived from multiple T_2 weighted spin–echo imaging techniques. Tritt-Goc and Pislewski (2002) acknowledged the fact that their images reflected T_{2app} rather than true T_2. A change in solvent pH was found to affect the water ingress and the HPMC tablet swelling process. The water diffusion into the polymer at pH = 2 was found to be controlled by the polymer relaxation indicating a case II diffusion mechanism; at pH = 6, a Fickian diffusion was observed. Furthermore, the polymer was found to swell to a greater extent in the radial direction at pH = 6 than at pH = 2.

Baumgartner et al. (2005) used a combination of standard spin–echo magnetic resonance imaging and conventional T_1/T_2 relaxation NMR spectroscopy on reference samples to allow them to calculate the water concentration profiles in the gel layer of hydrophilic matrix tablets. The gel layer thickness of hydroxyethyl cellulose (HEC), hydroxypropyl cellulose (HPC), and hydroxypropylmethyl cellulose (HPMC) (in the order of decreasing molecular weight) tablets were also measured. The thickness of the gel layer was found to be smaller in the matrix made of cellulose with lower molecular weight. It was concluded that, at a fixed time point, the difference in concentration profiles was due to the differences in characteristics of the polymer, i.e. the strength of the interactions between the polymer chains and polymer hydrophillicity. In addition Baumgartner et al. (2005) showed that it was possible to calculate the polymer concentration profile across the swollen layer of the tablet. The differences in the polymer concentration profiles after the same swelling time were attributed to the different characteristics of polymers themselves, i.e. different substitution type, molecular mass, hydrophillicity, polymer–water and polymer–polymer interactions.

Kowalczuk et al. (2004) studied the behaviour of the gel layer in HPMC matrices loaded with a different amount of the drug tetracycline hydrochoride. 2D multiple spin–echo pulse sequences based on the Hahn echo sequence was used for the MRI studies. The results showed that the drug loading decreased the resistance of the HPMC network structure against the movement of solvent molecules. The gel layer thickness and the rate of solvent penetration were found to increase with the increased amount of drug loaded in the matrix. In a similar study, Tritt-Goc and Kowalczuk (2005) used a 2D single-slice multi-echo pulse sequence based on a multiple-echo MRI imaging technique to investigate the spatially resolved alkaline solvent interaction with glassy HPMC polymer. Spatially resolved T_2 relaxation times and diffusion coefficients of the solvent molecules within the gel layer of HPMC samples, along with changes in the dimension of the glass core of the polymers were determined as a function of hydration times. The experimental data demonstrated that the transport diffusion mechanism as being Fickian and also allowed the mean diffusivity values of the

solvent molecules for each voxel within the gel of the studied polymers to be determined. It was found that the rate of gel layer growth and the extent of the tablet swelling increased with the increase of polymer molecular mass.

Dahlberg et al. (2007) used one dimensional constant time imaging(CTI≡SPI) (Emid and Creyghton, 1985; Gravina and Cory, 1994) to study the swelling characteristics of a hydroxypropyl methylcellulose (HPMC) matrix incorporating the hydrophilic drug antipyrine. This system was chosen to introduce a novel analytical method, which allowed them to obtain, within one experimental setup, information about the molecular processes of the polymer carrier and its impact on drug release. The imaging results revealed, *in situ*, the swelling behaviour of tablets when exposed to water. By using deuterated water, the spatial distribution and molecular dynamics of HPMC and their kinetics during swelling was observed selectively. In parallel, NMR spectroscopy provided the concentration of the drug released into the aqueous phase. Dahlberg et al. (2007) found that both swelling and release were diffusion controlled and concluded that monitoring these two processes, using the same experimental setup, facilitated the mapping of their interconnection, which highlighted the importance and potential of their analytical technique for further application in other drug delivery forms.

Recently, Laity et al. (2010) used a combination of T_1 and T_2 NMR relaxation spectroscopy, inversion nulling multiple-spin–echo MRI, and X-ray micro tomography to provide quantitative information concerning the movement of hydration fronts into HPMC tablets and the water content of the swollen gel layer, which formed at the tablet surface and progressively thickened with time. X-ray microtomography revealed significant axial expansion within the tablet core, at short times and ahead of the hydration fronts, where there was insufficient water to be observed by MRI which was estimated to be around 15% by weight for the system studied. Thus, Laity et al. (2010) concluded that both MRI and X-ray microtomography may be regarded as complementary methods for studying the hydration and swelling behaviour of tablets.

A new approach to combining different MRI methods has recently been reported by Mikac et al. (2010). In this study a combination of 1D single point imaging (Emid and Creyghton, 1985; Gravina and Cory, 1994) and 2D multi-echo MRI with T_2 mapping was used to give independent determination of penetration, swelling, and erosion front movement for different types of hydrophilic polymers. In comparison to previously published MRI studies, where swelling and penetration fronts were not distinguishable, Mikac et al. (2010) were able to accurately determine moving front positions and consequently the gel thickness, with higher precision. The penetration front was determined from 1D SPI profiles, the swelling front from the T_2 value of the maximally hydrated glassy polymer, and the erosion front from signal intensity profiles of 2D MRI. Mikac et al. (2010) showed that xanthan hydration depended on pH and ionic strength. Low pH and increased ionic strength were shown to influence xanthan molecular conformation, which constitutes the basis of xanthan bio-responsiveness and adoption of different structures under different micro-environmental conditions. However, these conformational differences were not reflected in the rate of gel formation, i.e. the swelling front position, which was the same for all six media. Xanthan bio-responsiveness was expressed under simulated physiological conditions, in which changes in medium conditions caused alterations at the molecular level, leading to relatively fast changes observed as macro scale effects. Mikac et al. (2010) concluded that drug release was regulated mainly by the structure of the xanthan gel, giving rise to different thicknesses of the gel layer.

Recently, Chen et al. (2010) gave the first report of a quantitative RARE based ultra-fast two-dimensional magnetic resonance imaging protocol to follow the water uptake of hydroxypropylmethyl cellulose (HPMC). Quantitative maps of absolute water concentration, T_2-spin–spin relaxation times and water self-diffusion coefficient, D, were obtained at a spatial resolution of 469 μm in less than 3 min each. These maps allowed the dynamic development of the medium release rate HPMC/water system to be followed. Figs. 13–15 show the quantitative water concentration images, T_2-relaxation maps and self-diffusion coefficients maps.

Chen et al. (2010) demonstrated that the evolution of the gel layer and, in particular, the gradient in water concentration across it, is significantly different when comparing the quantitative RARE sequence with a standard (non-quantitative) implementation of RARE. The total gel thickness in the axial direction grows faster than that in the radial direction and that the dry core initially expands anisotropically. Additionally, while HPMC was shown to absorb a large amount of water during the dissolution process, the concentration gradient of water within the gel layer was relatively small. Chen et al. (2010) presented the first ultra-fast MRI evidence for a transitional swollen glassy layer which resided between the outer edge of the dry tablet core and the inner edge of the gel layer.

5.3. Quantitative MRI studies of dynamic dissolution phenomena

This section aims to review some of the quantitative MRI work that has recently been published in the literature concerning the dissolution of pharmaceutically relevant devices. The previous two sections described results that generally concerned the uptake of a dissolution media in a static environment, which in general did not involve the complete dissolution of the polymer matrix. This section aims to review systems where the delivery matrix dissolves completely, and/or where the delivery matrix is in a flowing dissolution medium environment.

MRI has not only been used for investigating hydrogel matrix type drug release dosage forms, but also has been applied to other types of controlled drug delivery systems, such as osmotic pumps. Fahie et al. (1998) used a conventional 2D spin–echo MRI imaging technique to compare two types of regulated controlled release systems with the same formulation but different types of coating films. Whilst the ^{1}H magnitude images were not quantitative in terms of absolute ^{1}H spin density, quantitative information regarding the rate of ingress of dissolution medium could be gleaned from the images. The observation of the tablet dissolution processes in simulated USP gastric fluid without enzyme showed that the tablet with porous coating had a faster drug release rate than the non-porous one.

Tritt-Goc and Kowalczuk (2002) used the FLASH imaging (Haase et al., 1986) technique to study/compare the disintegration processes of paracetamol tablets produced by different pharmaceutical companies in acidic gastric pH solution (pH = 2) under temperature of 37 and 19 °C. A higher temperature was found to increase the rate of tablet disintegration.

Sutch et al. (2003) used a combination of 2D spin–echo and fast RARE (Hennig et al., 1986) MRI imaging techniques to elucidate the internal mechanisms underlying the different behaviours of pulsatile capsules coated with organic and aqueous processes. The premature drug release failure of the aqueous coated formulation during dissolution in water was found to be caused by the poor seal between the capsule and plug. Quantitative analysis of the MR images showed that the erosion kinetics of the plug was zero order.

Recently, more attention has been paid to studying dissolution phenomena with MRI under flowing conditions. Abrahmsén-Alami et al. (2007) studied the dimensional change of a swollen placebo hydrophilic polymer (polyethylene oxide (PEO)) tablet during dissolution process under solvent (water) flowing conditions using pulsed field gradient spin–echo MRI imaging technique. Faster rates of erosion and swelling were found in the radial direction than in the axial direction which was caused by the faster shear force

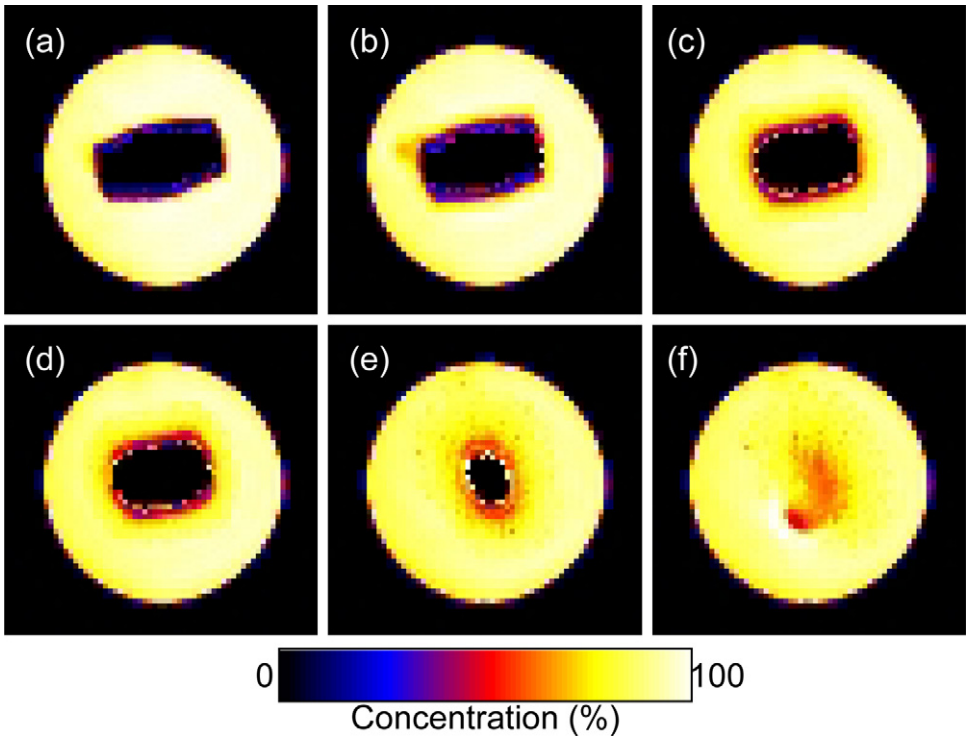

Fig. 13. Quantitative water concentration (C) maps of HPMC at different hydration times (hours): (a) 0.5; (b) 2; (c) 8; (d) 10.25; (e) 29.75; (f) 40.25. Reproduced with permission from reference (Chen et al., 2010).

in the radial direction when using a rotating disk set-up. Tajarobi et al. (2009) used the same experimental set-up of the flowing system, but applied multiple spin–echo pulse sequence to probe the swelling, erosion and dissolution of the HPMC tablet in phosphate buffer solution, and the effects of additives in the matrix on these processes. The dissolution rate was found to increase with the presence of more soluble additives, but the extent of the matrix swelling was found to be smaller.

Strübing et al. (2008) were amongst the first to use a bench-top MRI system to study water diffusion and swelling behaviour,

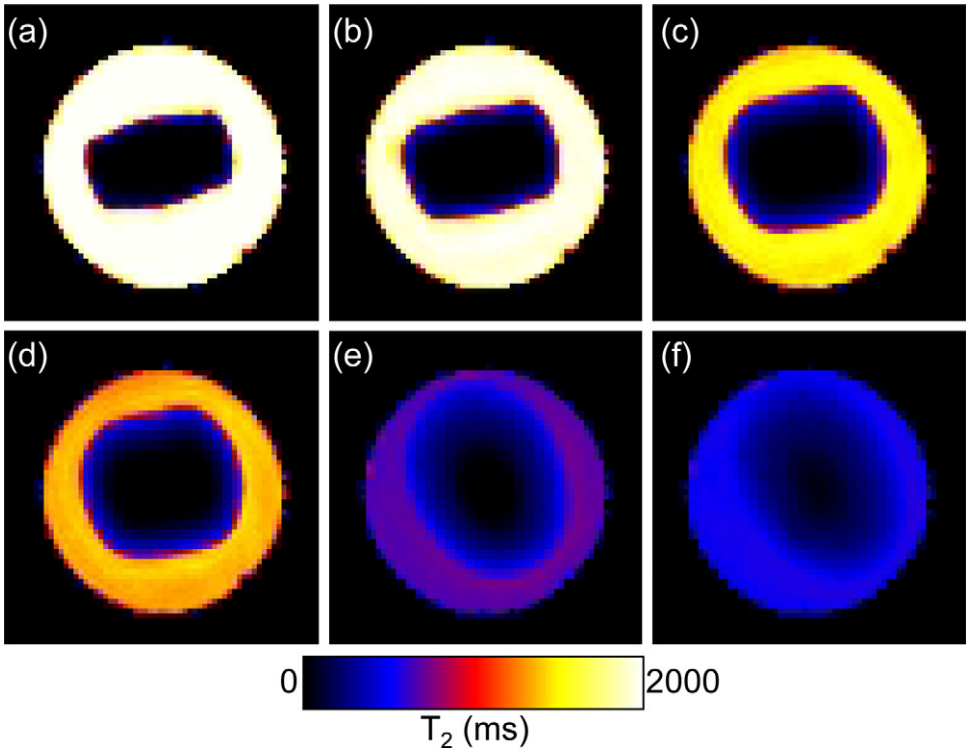

Fig. 14. T_2 relaxation maps of images in Fig. 13 at different hydration times (h): (a) 0.5; (b) 2; (c) 8; (d) 10.25; (e) 29.75; (f) 40.25. Reproduced with permission from reference (Chen et al., 2010).

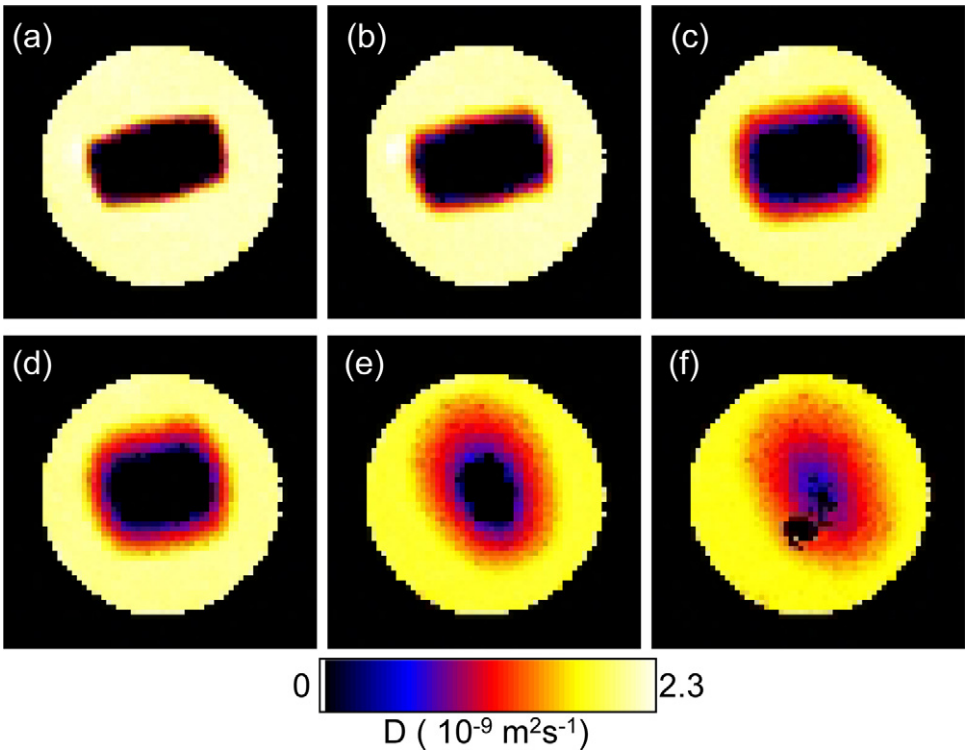

Fig. 15. Self-diffusion coefficient maps, *D*, at different hydration times (h): (a) 0.5; (b) 2; (c) 8; (d) 10.25; (e) 29.75; (f) 40.25. Reproduced with permission from reference (Chen et al., 2010).

non-invasively and continuously, in Kollidon® SR matrix tablets containing different amounts of Propranolol HCl. Strübing et al. (2008) performed the dissolution measurements ex-situ from the MRI system using a USP paddle dissolution apparatus. The samples were then removed from this apparatus and subsequently placed in the bench-top MRI apparatus at known times and scanned using standard spin–echo MRI. Fig. 16 shows a typical set of bench-top MRI images from (Strübing et al., 2008)(Strubing et al.'s, 2008) work for Kollidon® with a low (10%) drug loading.

Whilst absolute ^{1}H concentrations were not possible, collectively, the ^{1}H MR images revealed isotropic water diffusion for both low (10%) and high (33%) drug loaded samples. After 9 h the matrices were completely hydrated and the hydration of tablet samples with a higher drug content was expected to be faster due to rapid leaching of the hydrophilic model drug and a lower amount of matrix forming polymer hampering drug and water diffusion. Interestingly, Strübing et al. (2008) saw no significant difference in hydration velocity for either formulation. For tablets with a higher drug content after several hours of contact with dissolution medium, the visualization of the outer parts of the tablet matrix was decreased, so that only the inner core of the matrix tablet was visible. Strübing et al. (2008) attributed this to a possible higher

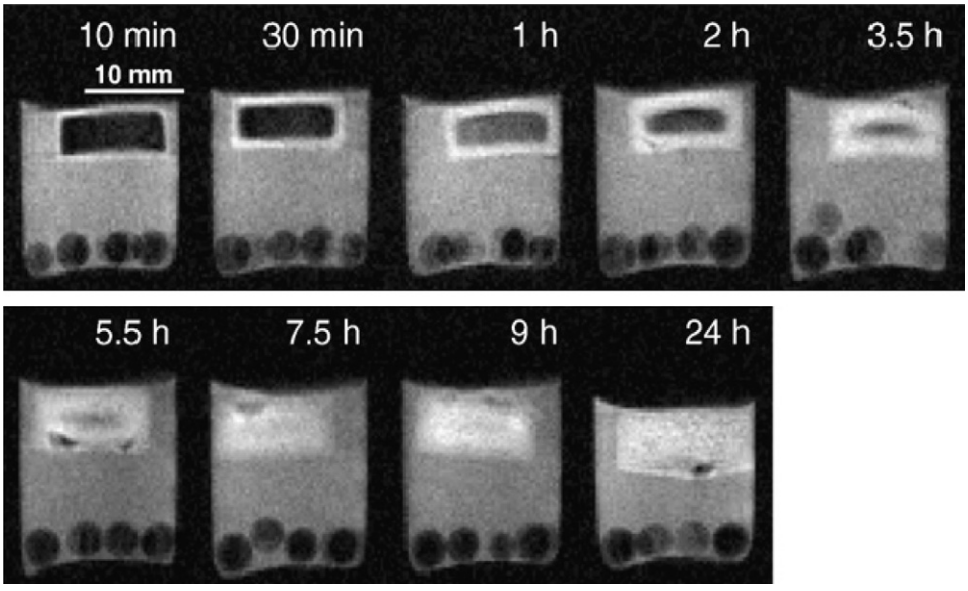

Fig. 16. Water penetration into matrix tablets with 10% propranolol HCl in 0.1 N HCl as a function of time. Reproduced with permission from reference (Strübing et al., 2008).

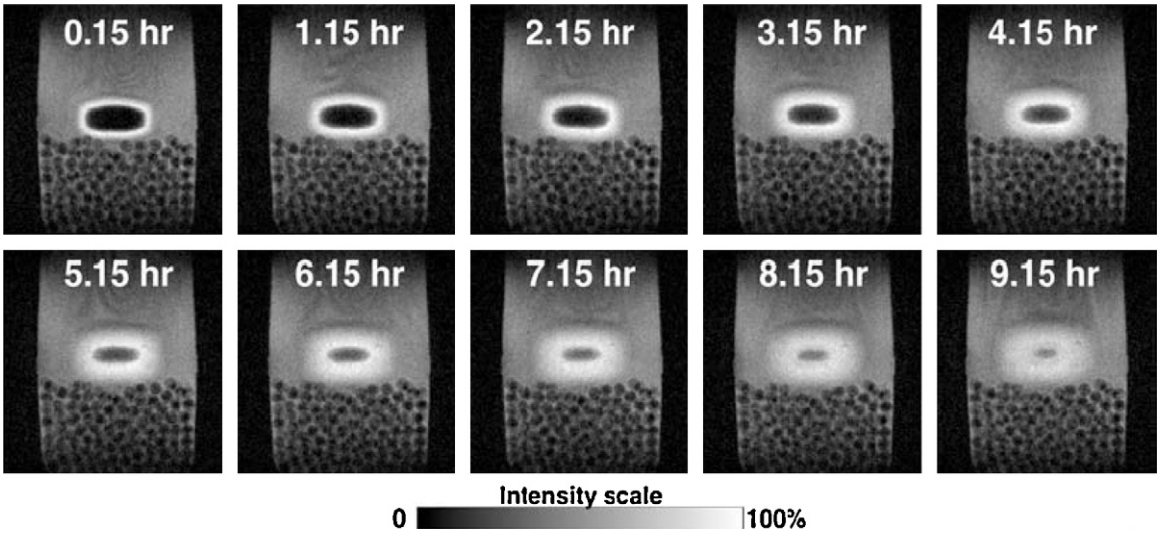

Fig. 17. A set of images acquired during dissolution of a chlorpheniramine maleate, USP standard tablet in water flowing at 16 ml/min at 37 °C in a closed loop configuration. Time stated is the start of a 4.3 min scan at 250-μm isometric pixel resolution and 3-mm slice (other image parameters: 12 ms echo time, 1 s repetition time and 2 averages). Reproduced with permission from reference (Nott, 2009).

porosity and a slight erosion in these areas of the matrix, resulting in a sponge-like structure with high amounts of dissolution medium inside the matrix.

Kulinowski et al. (2008) used a 2D flow compensated spin–echo MRI pulse sequence to compare the hydration processes of a hydrodynamically balanced (HB) dosage form in two types of simulated *in vivo* conditions with regard to temperature, volume, state and composition of dissolution media, and their drug release processes. A specially designed flow cell was constructed so that the dissolution MRI study could be done *in situ*. Whilst absolute ^{1}H spin density evaluation (and thus dissolution medium concentration) was not possible the images were analysed to give quantitative information regarding the time evolution of the hydrogel. In a similar study (Dorożyński et al., 2010) used the same MRI pulse sequence and solvent flowing experimental set-up to study the effect of HPMC grade on the HB tablet dissolution process in 0.1 M HCL solution. Although similar dissolution profiles of the drug were found, the imaging analysis revealed differences in the structural and geometrical changes of the HB tablet.

Malaterre et al. (2009) have recently used a bench-top MRI system, incorporating T_1 weighted spin–echo imaging, to study the swelling and hydrations kinetics of a push-pull osmotic system commonly called a gastrointestinal therapeutic system (GITS) (Shapiro et al., 1996). The critical parameters for the hydration balance were found to be the amount of drug loading, the presence of osmotic active agents and the molecular weight of the polymer matrix.

Therien-Aubin and Zhu (2009), recently showed that quantitative MR imaging of water uptake into starch based pharmaceutical tablets could be used to give the temporal evolution of the absolute water concentration profiles. In addition they showed that these profiles could be fitted to a Fickian diffusion equation based upon cylindrical geometry, thereby yielding the transport diffusivity.

Nott (2009) published the first results describing the dissolution of a chlorpheniramine drug loaded gel matrix tablet in a bench-top MRI system incorporating a standard USP-4 dissolution cell. In addition to the MRI results, the effluent stream of the flowing dissolution medium was passed to a UV analyser for online drug content analysis thereby enabling a direct comparison of quantitative drug release from the UV results with the swelling behaviour of the tablet from the MRI images.

Fig. 17 shows a series of images at different stages of dissolution under flowing conditions of a USP standard gel matrix tablet with chlorpheniramine maleate as the active ingredient using water flowing at 16 ml/min and 37 °C. A bed of glass beads were placed in the cone of the flow cell to ensure laminar flow further upstream and also to position the tablet without restricting the swelling. The rate of water ingress and swelling was quantified by calculating the areas of the non-hydrated core and whole tablet, respectively; the gel layer could also be quantified by subtracting one from the other. The boundary between the gel layer and the dissolution media was chosen by varying the contour intensity to highlight the tablet for a series of images until the gel layer becomes so diffuse that it becomes impossible to define; in practice, this was found to occur in a narrow window. The boundary between hydrated and non-hydrated regions was chosen by using a contour intensity that was half way between the highest (gel) and the lowest (non-hydrated core) intensities for the first image, which was used throughout the series.

Shiko et al. (2010) have recently present a detailed study of dissolution media hydrodynamics inside a flow-through dissolution apparatus when operated according to USP recommendations. The pulsatile flow inside the flow-through cell was measured quantitatively using magnetic MRI velocimetry (Mantle and Sederman, 2003) at a spatial resolution of $234 \times 234\ \mu m^2$ and slice thickness of 1 mm. Shiko et al. (2010) described the experimental protocols developed for *in situ* MRI studies and the effect that the operating conditions and tablet orientation have on the hydrodynamics inside a commercial USP-4 flow cell. Shiko et al. (2010) described how it was essential to acquire the MRI velocity images at exactly the same point in time for a particular phase of the USP-4 pump cycle. This was achieved by an optical triggering device between the pump and the MRI spectrometer. Fig. 18 shows MRI V_z-velocity maps, taken at three different points in the pump phase, for a USP-4 dissolution cell at two different flow rates, which represented the extremes recommended by the USP dissolution protocols.

It was found that the flow field inside the dissolution cells was, at most operating conditions, heterogeneous, rather than fully developed laminar flow, and was characterised by recirculation and backward flow. Fig. 19 shows the MRI V_z-velocity map taken during the flow of dissolution media around a non-dissolving bluff body tablet for three different phases of the dissolution pump cycle and for two different flow rates of 4.0 ml min^{-1} and 16 ml min^{-1}.

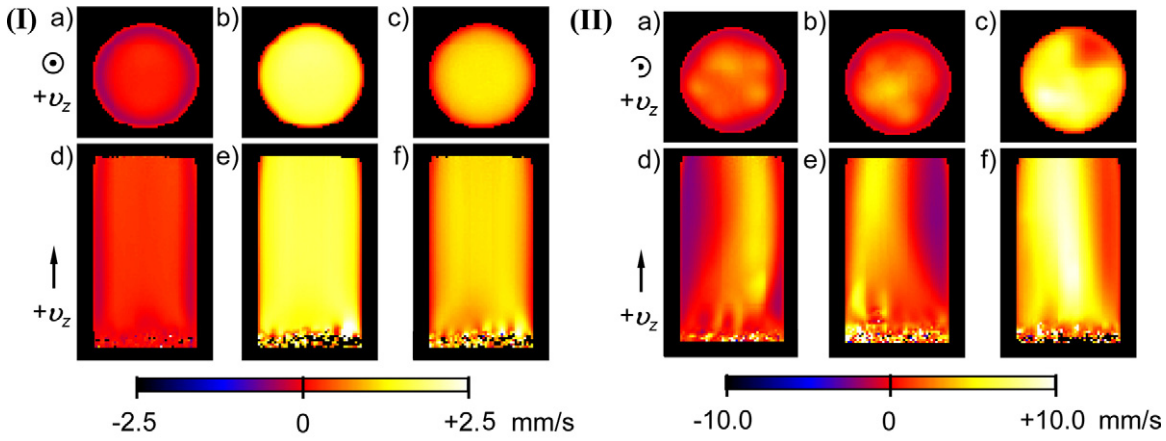

Fig. 18. (I). Time-averaged, phase-resolved velocity images of the axial velocity through the 12 mm USP-4 cell operating with liquid only at a flow rate of 4 mL/min and acquired at a pump phase of (a) 111 ms, (b) 306 ms and (c) 417 ms for a 528 ms long pump stroke. Cross-sectional images show axial velocity at an offset of + 3 mm from the 1 mm beads (a–c). (II) Time-averaged, phase-resolved velocity images of the axial velocity through the 12 mm USP 4 cell operating with liquid only at a flow rate of 16 mL/min and acquired at a pump phase of (a) 83.3 ms, (b) 111 ms and (c) 306 ms for a 528 ms long pump stroke. For (I) and (II) longitudinal images show axial velocity through the middle of the flow-through cell (d–f). All images have a resolution of 230 × 230 μm^2 for a 1 mm thick imaging slice. Reproduced with permission from reference (Shiko et al., 2010).

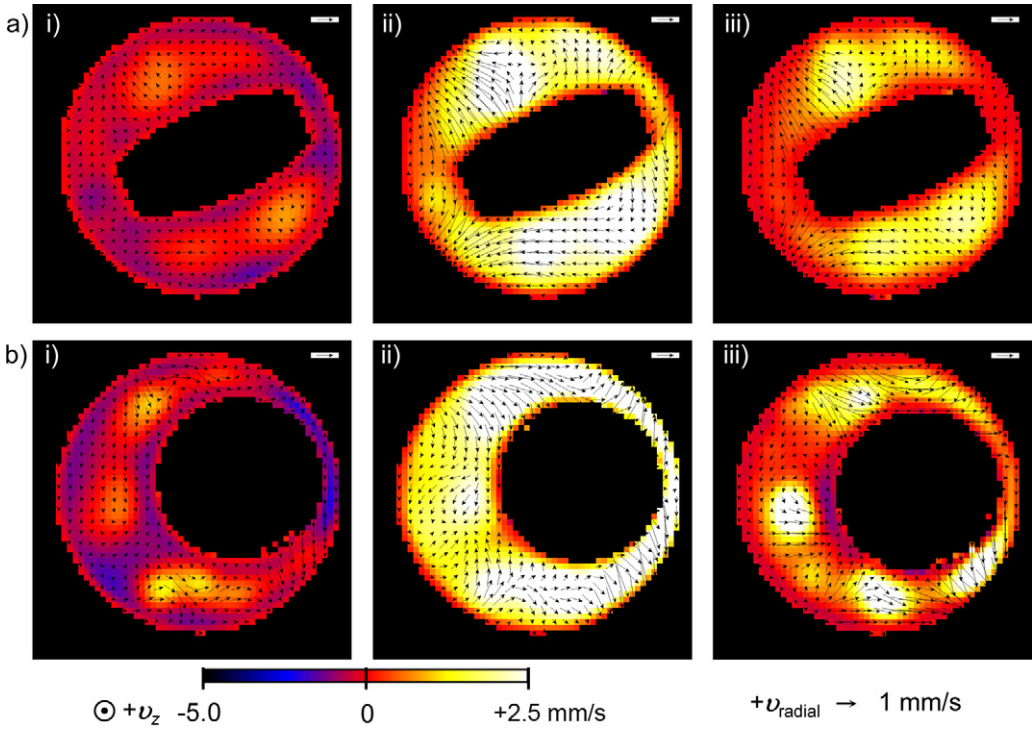

Fig. 19. Time-averaged, phase-resolved velocity images of the axial and radial velocities around a model non-disintegrating tablet when (a) held vertically and (b) placed horizontally on the 1 mm beads. All images were acquired in the 12 mm i.d. USP-4 cell operating at 8 mL/min and at a pump phase of (i) 83.3 ms, (ii) 306 ms, and (iii) 472 ms for a 528 ms long pump stroke. The colour scale corresponds to the axial velocity. The vector scale corresponds to the magnitude and direction of radial velocity. Images were acquired at offsets of +7 and + 3 mm for the vertically and horizontally placed tablets, respectively. All images have a resolution of 230 × 230 μm^2 for a 1 mm thick imaging slice. Reproduced with permission from reference (Shiko et al., 2010).

Fig. 19 clearly shows that the model tablet was contacted by a wide distribution of local velocities as a function of position and orientation in the flow cell. The use of 1 mm beads (specified by USP protocols) acted as a distributor of the flow but did not suffice to ensure a fully developed laminar flow profile. Shiko et al.'s (2010) results emphasised the necessity to understand the influence of test conditions on dissolution behaviour in defining robust flow-through dissolution methods.

6. Summary remarks

The aim of this review (and the supplementary material) was firstly to describe in some detail the theoretical basis behind NMR/MRI signal quantitation and how one must consider the effects of T_1 and T_2 relaxation and diffusion in order to obtain optimised quantitative results. A second aim was to give some relatively simple guidelines to aid the experimentalist in choos-

ing/identifying suitable MRI protocol(s) for pharmaceutically relevant research. A current review of the literature showed that conventional (spin–echo) quantitative magnetic resonance techniques can be applied to both non-swelling and swelling pharmaceutically relevant polymer systems to give absolute species concentration, species self- and transport mobility and matrix pore size evolution, provided that T_1 and T_2-relxation and diffusive losses of the signal can be accounted for. In cases where this is not possible, semi-quantitative information can still be gleaned from MRI data, usually in the form of gel swelling kinetics and/or the transport behaviour of the penetration fronts of the dissolution media. In addition, it was shown that fast (minutes or less) magnetic resonance imaging techniques could also be used to quantify the dissolution behaviour of pharmaceutical systems that change over tens of minutes to hours. The quantification of dissolution media hydrodynamics in a USP-4 standard dissolution apparatus (previously thought to be 'laminar' under standard operating condition) has recently been achieved using MRI velocimetry and is likely to give new insights into correlating standard offline UV measurements of drug release with the internal hydrodynamics of the USP-4 dissolution cell.

It is likely, in the next 5–10 years, that all industrial pharmaceutical research laboratories will be equipped with some form of bench-top MRI spectrometer that is dedicated to facilitate the understanding of drug matrix dissolution phenomena. However, because of the strict protocols associated with standard methods of dissolution testing, in order for the MRI data to be accepted as meaningful, it will become increasingly important to account for any 'MRI signal anomalies' that arise from the technique itself. Perhaps the ultimate goal of the MRI research tool in a pharmaceutical setting is, at the push of a button, to be able to fully quantify from start to finish the following: the spatial distribution of API in the solid dosage form; the dynamic dissolution of the matrix in terms of diffusion front ingress and water concentration; the dynamic, spatially resolved, evolution of drug mass transfer to include rate of dissolution and subsequent transport out of the delivery device into the flowing dissolution medium; the porosity evolution of delivery matrix during dissolution; the chemical behaviour of the API during dissolution using localised NMR spectroscopy; relating the hydrodynamics of the dissolution medium to drug release profiles. Clearly, we are not there yet, but the advent of commercially available cheaper bench-top MRI spectrometers complemented by traditional high field NMR/MRI research, will provide an ever increasing data base and thus the rate at which the 'ultimate goal', as far as MRI and pharmaceutical research is concerned, will, hopefully, accelerate in the future.

Acknowledgements

MDM wishes to thank Dr Andrew Sederman for useful discussions during the preparation of this review.

Appendix A. Supplementary data

Supplementary data associated with this article can be found, in the online version, at doi:10.1016/j.ijpharm.2010.11.035.

References

Abrahmsén-Alami, S., Körner, A., Nilsson, I., Larsson, A., 2007. New release cell for NMR microimaging of tablets: swelling and erosion of poly(ethylene oxide). Int. J. Pharm. 342, 105–114.

Ashraf, M., Iuorno, V.L., Coffinbeach, D., Evans, C.A., Augsburger, L.L., 1994. A novel nuclear-magnetic-resonance (NMR) imaging method for measuring the water front penetration rate in hydrophilic polymer matrix capsule plugs and its role in drug-release. Pharm. Res. 11, 733–737.

Baumgartner, S., Lahajnar, G., Sepe, A., Kristl, J., 2005. Quantitative evaluation of polymer concentration profile during swelling of hydrophilic matrix tablets using H-1 NMR and MRI methods. Eur. J. Pharm. Biopharm. 59, 299–306.

Bowtell, R., Sharp, J.C., Peters, A., Mansfield, P., Rajabisiahboomi, A.R., Davies, M.C., Melia, C.D., 1994. NMR microscopy of hydrating hydrophilic matrix pharmaceutical tablets. Mag. Reson. Imaging 12, 361–364.

Brandl, M., Haase, A., 1994. Molecular-diffusion in NMR microscopy. J. Mag. Reson. Ser. B 103, 162–167.

Callaghan, P.T., 1993. Principles of Nuclear Magnetic Resonance Microscopy. Oxford University Press, New York.

Carr, H.Y., Purcell, E.M., 1954. Effects of diffusion on free precession in nuclear magnetic resonance experiments. Phys. Rev. 94, 630–638.

Chen, Q., Kinzelbach, W., Oswald, S., 2002. Nuclear magnetic resonance imaging for studies of flow and transport in porous media. J. Environ. Qual. 31, 477–486.

Chen, 2010. Quantitative ultrafast magnetic resonance imaging studies of controlled release pharmaceuticals, Ph.D. thesis, University of Cambridge, England, U.K, 2010.

Chen, Y.Y., Hughes, L.P., Gladden, L.F., Mantle, M.D., 2010. Quantitative ultra-fast MRI of HPMC swelling and dissolution. J. Pharm. Sci. 99, 3462–3472.

Chowdhury, M.A., Hill, D.J.T., Whittaker, A.K., 2004. NMR imaging of the diffusion of water at 37 °C into poly(2-hydroxyethyl methacrylate) containing aspirin or vitamin B-12. Biomacromolecules 5, 971–976.

Collins, J.H.P., Gladden, L.F., Hardy, I.J., Mantle, M.D., 2007. Characterizing the evolution of porosity during controlled drug release. Appl. Magn. Reson. 32, 185–204.

Cotts, R.M., Hoch, M.J.R., Sun, T., Markert, J.T., 1989. Pulsed field gradient stimulated echo methods for improved NMR diffusion measurements in heterogeneous systems. J. Magn. Reson. 83, 252–266.

Dahlberg, C., Fureby, A., Schuleit, M., Dvinskikh, S.V., Furó, I., 2007. Polymer mobilization and drug release during tablet swelling. A 1H NMR and NMR microimaging study. J. Controlled Release 122, 199–205.

Djemai, A., Gladden, L.F., Booth, J., Kittlety, R.S., Gellert, P.R., 2001. MRI investigation of hydration and heterogeneous degradation of aliphatic polyesters derived from lactic and glycolic acids: a controlled drug delivery device. Magn. Reson. Imaging 19, 521–523.

Djemai, A., Sinka, I.C., 2006. NMR imaging of density distributions in tablets. Int. J. Pharm. 319, 55–62.

Dorożyński, P., Kulinowski, P., Mendyk, A., Młynarczyk, A., Jachowicz, R., 2010. Novel application of MRI technique combined with flow-through cell dissolution apparatus as supportive discriminatory test for evaluation of controlled release formulations. AAPS PharmSciTech 11, 588–597.

Emid, S., Creyghton, J.H.N., 1985. High-resolution NMR imaging in solids. Physica B & C 128, 81–83.

Fahie, B.J., Nangia, A., Chopra, S.K., Fyfe, C.A., Grondey, H., Blazek, A., 1998. Use of NMR imaging in the optimization of a compression-coated regulated release system. J. Controlled Release 51, 179–184.

Fyfe, C.A., Blazek-Welsh, A.I., 2000. Quantitative NMR imaging study of the mechanism of drug release from swelling hydroxypropylmethylcellulose tablets. J. Controlled Release 68, 313–333.

Fyfe, C.A., Blazek, A.I., 1997. Investigation of hydrogel formation from hydroxypropylmethylcellulose (HPMC) by NMR spectroscopy and NMR imaging techniques. Macromolecules 30, 6230–6237.

Gao, P., Fagerness, P.E., 1995. Diffusion in HPMC gels 1. Determination of drug and water diffusivity by pulsed-field-gradient spin-echo NMR. Pharm. Res. 12, 955–964.

Gravina, S., Cory, D.G., 1994. Sensitivity and resolution of constant-time imaging. J. Magn. Reson. Ser. B 104, 53–61.

Haacke, E.M., 1999. Magnetic Resonance Imaging: Physical Principles and Sequence Design. John Wiley and Sons.

Haase, A., Frahm, J., Matthaei, D., Hanicke, W., Merboldt, K.D., 1986. Flash imaging – rapid NMR imaging using low flip-angle pulses. J. Magn. Reson. 67, 258–266.

Hahn, E.L., 1950. Spin echoes. Phys. Rev. 80, 580–594.

Harding, S., Baumann, H., Gren, T., Seo, A., 2000. NMR microscopy of the uptake, distribution and mobility of dissolution media in small, sub-millimetre drug delivery systems. J. Controlled Release 66, 81–99.

Hennig, J., 1988. Multiecho imaging sequences with low refocusing flip angles. J. Magn. Reson. 78, 397–407.

Hennig, J., 1991. Echoes-how to generate, recognize. Use or avoid them in MR-imaging sequences. Part I: fundamental and nor so fundamental properties of spin echoes. Concepts Magn. Reson. 3, 125–143.

Hennig, J., Nauerth, A., Feiedburg, H., 1986. Rare imaging: a fast method for clinical MR. Magn. Reson. Med. 3, 823–833.

Hennig, J., Weigel, M., Scheffler, K., 2003. Multiecho sequences with variable refocusing flip angles: optimization of signal behavior using smooth transitions between pseudo steady states (TRAPS). Magn. Reson. Med. 49, 527–535.

Hennig, J., Weigel, M., Scheffler, K., 2004. Calculation of flip angles for echo trains with predefined amplitudes with the extended phase graph (EPG)-algorithm: principles and applications to hyperecho and TRAPS sequences. Magn. Reson. Med. 51, 68–80.

Howseman, A.M., Stehling, M.K., Chapman, B., Coxon, R., Turner, R., Ordidge, R.J., Cawley, M.G., Glover, P., Mansfield, P., Coupland, R.E., 1988. Improvements in snap-shot nuclear magnetic-resonance imaging. Br. J. Radiol. 61, 822–828.

Hsu, E.W., Schoeniger, J.S., Bowtell, R., Aiken, N.R., Horsman, A., Blackband, S.J., 1995. A modified imaging sequence for accurate T-2 measurements using NMR microscopy. J. Magn. Reson. Ser. B 109, 66–69.

Hurlimann, M.D., 1998. Effective gradients in porous media due to susceptibility differences. J. Magn. Reson. 131, 232–240.

Hyde, T.M., Gladden, L.F., 1998. Simultaneous measurement of water and polymer concentration profiles during swelling of poly(ethylene oxide) using magnetic resonance imaging. Polymer 39, 811–819.

Hyde, T.M., Gladden, L.F., Mackley, M.R., Gao, P., 1995a. Quantitative nuclear-magnetic-resonance imaging of liquids in swelling polymers. J. Polym. Sci. Part A – Polym. Chem. 33, 1795–1806.
Hyde, T.M., Gladden, L.F., Payne, R., 1995b. A nuclear magnetic resonance imaging study of the effect of incorporating a macromolecular drug in poly(glycolic acid-co-DL-lactic acid). J. Controlled Release 36, 261–275.
Karakosta, E., McDonald, P.J., 2007. An MRI analysis of the dissolution of a soluble drug incorporated within an insoluble polymer tablet. Appl. Magn. Reson. 32, 75–91.
Kowalczuk, J., Tritt-Goc, J., Pislewski, N., 2004. The swelling properties of hydroxypropyl methyl cellulose loaded with tetracycline hydrochloride: magnetic resonance imaging study. Solid State Nucl. Magn. Reson. 25, 35–41.
Kulinowski, P., Dorozynski, P., Jachowicz, R., Weglarz, W.P., 2008. An integrated system for dissolution studies and magnetic resonance imaging of controlled release, polymer-based dosage forms – a tool for quantitative assessment of hydrogel formation processes. J. Pharm. Biomed. Anal. 48, 685–693.
Laity, P.R, Mantle, M.D., Gladden, L.F., Cameron, R.E., 2010. Magnetic resonance imaging and X-ray microtomography studies of a gel-forming tablet formulation. Eur. J. Pharm. Biopharm. 74, 109–119.
Leroux, P., Hinks, R.S., 1993. Stabilization of echo amplitudes in FSE sequences. Magn. Reson. Med. 30, 183–190.
Levitt, M.H., 2001. Spin Dynamics: Basics of Nucelar Magnetic Resonance. John Wiley and Sons.
Liang, Z.P., Lauterbur, P.C., 2000. Principles of Magnetic Resonance Imaging: a signal processing perspective. IEEE Press Series in Biomedical Engineering.
Madhu, B., Hjartstam, J., Soussi, B., 1998. Studies of the internal flow process in polymers by H 1 NMR microscopy at 500 MHz. J. Controlled Release 56, 95–104.
Malaterre, V., Metz, H., Ogorka, J., Gurny, R., Loggia, N., Mader, K., 2009. Benchtop-magnetic resonance imaging (BT-MRI) characterization of push-pull osmotic controlled release systems. J. Controlled Release 133, 31–36.
Mansfield, P., 1977. J. Phys. C 10, L55–L58.
Mansfield, P., Grannell, P.K., 1973. J. Phys. C 6, L422–426.
Mantle, M.D., Sederman, A.J., 2003. Dynamic MRI in chemical process and reaction engineering. Prog. Nucl. Magn. Reson. Spectrosc. 43, 3–60.
Meiboom, S., Gill, D., 1958. Modified spin-echo method for measuring nuclear relaxation times. Rev. Sci. Instrum. 29, 688–691.
Melia, C.D., Rajabi-Siahboomi, A.R., Bowtell, R.W., 1998. Magnetic resonance imaging of controlled release pharmaceutical dosage forms. Pharm. Sci. Technol. Today 1, 32–39.
Mikac, U., Sepe, A., Kristl, J., Baumgartner, S., 2010. A new approach combining different MRI methods to provide detailed view on swelling dynamics of xanthan tablets influencing drug release at different pH and ionic strength. J. Controlled Release 145, 247–256.
Norris, D.G., Bornert, P., 1993. Coherence and interference in ultrafast rare experiments. J. Magn. Reson. Ser. A 105, 123–127.
Norris, D.G., Bornert, P., Reese, T., Leibfritz, D., 1992. On the application of ultra-fast rare experiments. Magn. Reson. Med. 27, 142–164.
Nott, K.P., 2009. Magnetic resonance imaging of tablet dissolution. Eur. J. Pharm. Biopharm. 74, 78–83.
Nott, K.P., 2010. Magnetic resonance imaging of tablet dissolution. Eur. J. Pharm. Biopharm. 74, 78–83.
Pitkin, C., Carstens, J., 1973. Moisture content of granulations. J. Pharm. Sci. 62, 1215–11215.
Rajabi-Siahboomi, A.R., Bowtell, R.W., Mansfield, P., Davies, M.C., Melia, C.D., 1996. Structure and behavior in hydrophilic matrix sustained release dosage forms: 4. Studies of water mobility and diffusion coefficients in the gel layer of HPMC tablets using NMR imaging. Pharm. Res. 13, 376–380.
Rajabisiahboomi, A.R., Bowtell, R.W., Mansfield, P., Henderson, A., Davies, M.C., Melia, C.D., 1994. Structure and behavior in hydrophilic matrix sustained-release dosage forms.2. NMR-imaging studies of dimensional changes in the gel layer and core of HPMC tablets undergoing hydration. J. Controlled Release 31, 121–128.
Richardson, J.C., Bowtell, R.W., Mader, K., Melia, C.D., 2005. Pharmaceutical applications of magnetic resonance imaging (MRI). Adv. Drug Deliv. Rev. 57, 1191–1209.
Schick, F., 1997. SPLICE: sub-second diffusion-sensitive MR imaging using a modified fast spin-echo acquisition mode. Magn. Reson. Med. 38, 638–644.
Sederman, A.J., Mantle, M.D., Gladden, L.F., 2003. Single excitation multiple image RARE (SEMI-RARE): ultra-fast imaging of static and flowing systems. J. Magn. Reson. 161, 15–24.
Shapiro, M., Jarema, M.A., Gravina, S., 1996. Magnetic resonance imaging of an oral gastrointestinal-therapeutic-system (GITS) tablet. J. Controlled Release 38, 123–127.
Shiko, G., Gladden, L.F., Sederman, A.J., Connoly, P.C., Butler, J.M., 2010. MRI studies of the hydrodynamics in a USP 4 dissolution testing cell. Journal of Pharmaceutical Sciences, doi:10.1002/jps.22343.
Stejskal, E.O., Tanner, J.E., 1965. J. Chem. Phys. 42, 288–292.
Strübing, S., Metz, H., Mäder, K., 2008. Characterization of poly(vinyl acetate) based floating matrix tablets. J. Controlled Release 126, 149–155.
Sutch, J.C.D., Ross, A.C., Kockenberger, W., Bowtell, R.W., MacRae, R.J., Stevens, H.N.E., Melia, C.D., 2003. Investigating the coating-dependent release mechanism of a pulsatile capsule using NMR microscopy. J. Controlled Release 92, 341–347.
Tajarobi, F., Abrahmsén-Alami, S., Carlsson, A.S., Larsson, A., 2009. Simultaneous probing of swelling, erosion and dissolution by NMR-microimaging – effect of solubility of additives on HPMC matrix tablets. Eur. J. Pharm. Sci. 37, 89–97.
Therien-Aubin, H., Zhu, X.X., 2009. NMR spectroscopy and imaging studies of pharmaceutical tablets made of starch. Carbohyd. Polym. 75, 369–379.
Tritt-Goc, J., Kowalczuk, J., 2002. In situ, real time observation of the disintegration of paracetamol tablets in aqueous solution by magnetic resonance imaging. Eur. J. Pharm. Sci. 15, 341–346.
Tritt-Goc, J., Kowalczuk, J., 2005. Spatially resolved solvent interaction with glassy HPMC polymers studied by magnetic resonance microscopy. Solid State Nucl. Magn. Reson. 28, 250–257.
Tritt-Goc, J., Pislewski, N., 2002. Magnetic resonance imaging study of the swelling kinetics of hydroxypropylmethylcellulose (HPMC) in water. J. Controlled Release 80, 79–86.
Zeitler, J.A., Gladden, L.F., 2009. In-vitro tomography and non-destructive imaging at depth of pharmaceutical solid dosage forms. Eur. J. Pharm. Biopharm. 71, 2–22.
Zur, Y., 2004. An algorithm to calculate the NMR signal of a multi spin-echo sequence with relaxation and spin-diffusion. J. Magn. Reson. 171, 97–106.